ORKUSTOFNUN
NATIONAL ENERGY AUTHORITY
GEOTHERMAL DIVISION

Jan A Czubek

INSTITUTE OF NUCLEAR PHYSICS
ul. Radzikowskiego 152
31 - 342 Krakow, Poland.

SOME ASPECTS ON NUCLEAR WELL LOGGING IN IGNEOUS ROCK

Notes on lectures presented by J. A. Czubek in June 1978 at Orkustofnun, Iceland, as a part of the International Atomic Energy Agency, Project ICE/8/02

OS81009/JHD05
Reykjavík, June 1981

ORKUSTOFNUN
NATIONAL ENERGY AUTHORITY
GEOTHERMAL DIVISION
GRENSÁSVEGUR 9,
108 REYKJAVÍK ICELAND

Jan A Czubek

INSTITUTE OF NUCLEAR PHYSICS
ul. Radzikowskiego 152
31 - 342 Krakow, Poland.

SOME ASPECTS ON NUCLEAR WELL LOGGING IN IGNEOUS ROCK

Notes on lectures presented by J. A. Czubek in June 1978 at Orkustofnun, Iceland, as a part of the International Atomic Energy Agency, Project ICE/8/02

OS81009/JHD05
Reykjavík, June 1981

PREFACE

The International Atomic Energy Agency in Vienna sponsored the introduction of nuclear well logging in geothermal investigations in Iceland.

In that connection Professor Jan A. Czubek's experts mission to Iceland in June 1978 was an invaluable contribution. Prof. Czubek demonstrated his wide and deep knowledge in nuclear logging, and this mission led to the practising of a new successful investigation method in geothermal logging in this country. During a training program in June 1978, Professor Czubek presented informal lectures where the basic concepts of the gamma-ray and neutron log intepretation were reviewed.

When training in geothermal logging,as a part of the Geothermal Training Programme at the United Nations University in Reykjavík started, Professor Czubek's lecture notes from 1978 again became a popular reference manual, and the need for publishing the lectures became urgent.

Sincere thanks are due to Professor Czubek for his enthusiastic introduction to nuclear logging as well as his continuous interest and help during the progress of this discipline in Iceland.

Reykjavík in August 1981

Valgarður Stefánsson

LIST OF CONTENTS

1 HOW TO CHOOSE THE BEST PARAMETERS FOR THE LOG RECORD (RATEMETER CASE)

1 HOW TO CHOOSE THE BEST PARAMETERS FOR THE LOG RECORD (RATEMETER CASE)

J.A.C. JUNE 6, 1978

When the nuclear log is recorded with the ratemeter, the parameters needed to be chosen for its proper record, are:

ν - logging speed

RC - ratemeter time constant

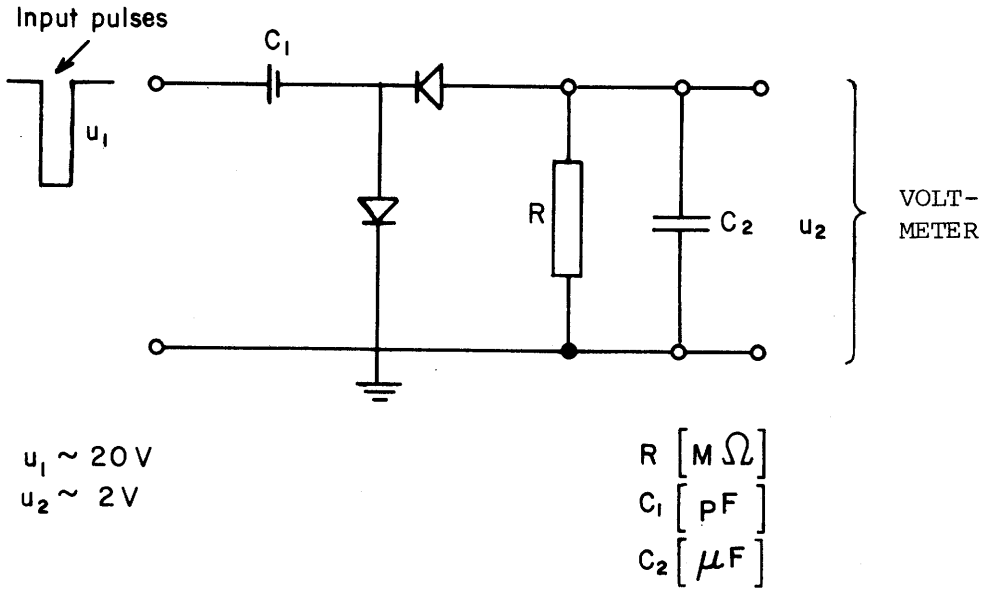

Fig. 1

Ratemeter

When $u_2 << u_1$ one has in the equilibrium conditions

$u_2 \sim I$, where

I is the constant pulse rate at the input. When the input pulse rate I is variable, let us say I(t), one has to consider the constant logging speed ν, in this case

$$z = t \cdot \nu, \qquad (1)$$

where t is the time, and z is the depth along the borehole. When the "output" intensity at the ratemeter is denoted J(t), one has in this case:

$$J(t) = \frac{1}{RC} \cdot e^{-\frac{t}{RC}} \int_0^t e^{\frac{t'}{RC}} I(t')\, dt' \qquad (2)$$

or

$$I(t) = J(t) + RC \frac{d\,J(t)}{dt} \qquad (3)$$

Both, eqs. 2 and 3 are the ratemeter equations, which in the case of logging, taking into account eq. (1), are:

$$J(z) = \frac{1}{v.RC}\, e^{-\frac{2}{vRC}} \int_{-\infty}^{z} I(z')\, e^{\frac{z'}{vRC}}\, dz' \qquad (4)$$

or

$$I(z) = J(z) + v.RC \frac{d\,J(z)}{dz} \qquad (5)$$

We call I(z) the static anomaly, and J(z) the dynamic anomaly which are schematically presented in fig. 2.

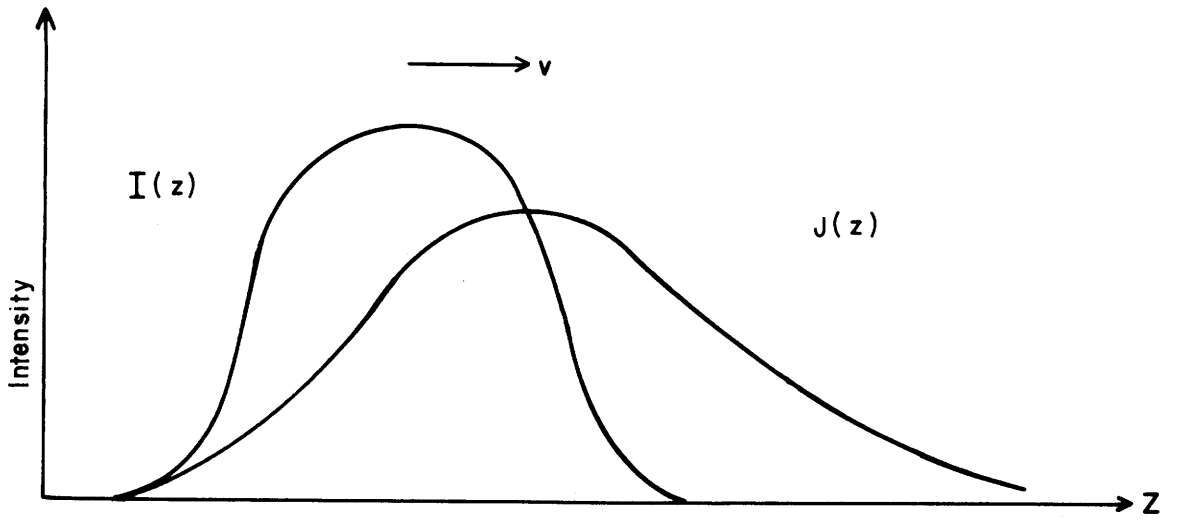

Fig. 2

As it is clear from eq. 5 the maximum of the dynamic anomaly J(z) is always at the intersection with the static one, and one has the relation about the area under the curves:

$$S = \int_{-\infty}^{+\infty} I(z)\, dz = \int_{-\infty}^{+\infty} J(z)\, dz \tag{6}$$

In the case of the gamma-ray log there is also another relationship

$$S = H \cdot I_{\infty} \tag{7}$$

where H is the thickness of the radioactive layer, and I_{∞} is the gamma ray intensity when $H \to \infty$.

As a matter of fact I(z) is never a smooth function, it obeys to the statistical variation according to the Poisson law. In this case the variance of the output reading $J(z,\nu,RC)$ is:

$$\sigma^2\,[J(z,\nu,RC)] = \frac{1}{2 \cdot RC}\, J(z,\nu,\frac{RC}{2}) \tag{8}$$

which in the case

$$I(z) = \text{const} \tag{9}$$

gives for $t \gg o$

$$J(z,\nu RC) = I(z) = \text{const} \tag{10}$$

and

$$\sigma^2\,(J) = \frac{1}{2RC \cdot J} = \frac{1}{2 \cdot RC \cdot I}\,, \tag{11}$$

the formula known to any nuclear physicist.

When one takes, for the simplicity of considerations, the rectangular form of the static anomaly, i.e.

$$I(z) = \begin{cases} o & z \leq o \\ I & o \leq z \leq H \\ o & z \geq H \end{cases} \tag{12}$$

one has from eq. 4:

$$J(z) = \begin{cases} 0 & z \leq 0 \\ I\,(1-e^{-\frac{z}{\nu \cdot RC}}) & 0 \leq z \leq H \\ I\,(1-e^{-\frac{H}{\nu \cdot RC}}) \cdot e^{-\frac{z-H}{\nu \cdot RC}} & z \geq H \end{cases} \qquad (13)$$

Which is depicted in fig. 3

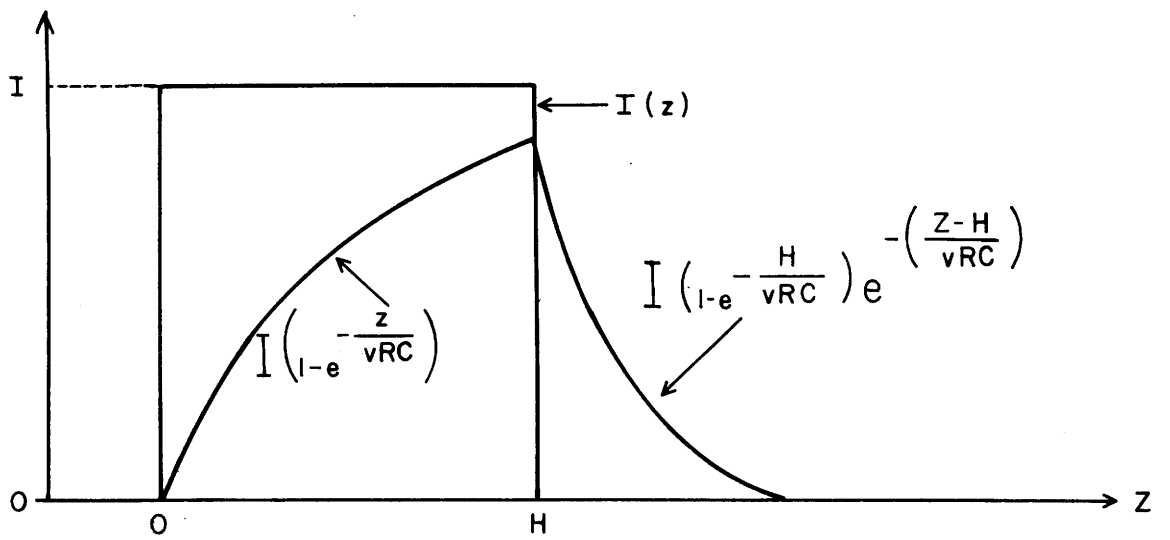

Fig. 3

The value of J(z) at its maximum is for z = H:

$$J(H) = I(1-e^{-\frac{H}{\nu RC}}) \qquad (14)$$

and the value

$$\Delta = \frac{I - J(H)}{I} = e^{-\frac{H}{\nu RC}} \qquad (15)$$

is called the dynamic distortion which we want to be as small as possible. Usually one takes $\Delta \approx 5\%$ or less.

As we can see from table 1 the probe should be at least during the time

equal to 3 time constants RC inside the layer to have the recorded maximum of the dynamic curve different from the true value not less than 5%. Thus, for the qualitative measurement one takes the value $H/(\nu RC)$

TABLE 1

$\frac{H}{\nu RC}$	$\Delta(\%)$
1.0	36.79
2.0	13.53
3.0	4.98
4.0	1.83
5.0	0.67

in the limits

$$2 \leq \frac{H}{\nu RC} \leq 3 \tag{16}$$

whereas, for the quantitative measurement one takes

$$\frac{H}{\nu RC} \geq 4. \tag{17}$$

Conditions (16) and (17) define the value of the lag $\nu \cdot RC$ in terms of the thickness of layer to be investigated. The minimum thickness H is for the gamma-ray log equal to the length L of the detector (in our case $L = 18" = 45.72$ cm) and in the case of the neutron or density log is equal to the source-detector spacing (in our case for the N.N. log):

$$\frac{L}{2} + 13" = 33.02 \text{ cm} + 10 \text{ cm} = \sim 43 \text{ cm}$$

$$L/2 + 15" = 38.10 \text{ cm} + 10 \text{ cm} = \sim 48 \text{ cm}$$

$$L/2 + 17" = 43.18 \text{ cm} + 10 \text{ cm} = \sim 53 \text{ cm}$$

and for density tool:

$$H_{min} = \sim 55 \text{ cm}$$

Thus, if one takes as an average

$$H_{min} \sim 50 \text{ cm}$$

one has for the qualitative measurement

$$\nu \cdot RC \approx 0.4 \quad H_{min} \approx 20 \text{ cm}$$

and for the quantitative measurement

$$\nu \cdot RC \approx 0.25 \; H_{min} = 12.5 \text{ cm}.$$

If, for some reasons (usually technical), one applies for example

$$\nu \; RC = 100 \text{ cm}$$

one can distinguish the thickness

$$H_{min} = 2.5 \; \nu RC = 2.5 \text{ m}$$

and one can measure quantitatively the layers with

$$H_{min} = 4 \; \nu RC = 4 \text{ m}.$$

Once the lag $\nu \cdot RC$ is selected the question is how to divide it into the logging velocity ν and the ratemeter time constant RC.

The RC value is chosen according to the accuracy demanded for measurement. From eq. (8) one has for the anomaly from fig. 3 that

$$\sigma^2 \left[J(z,\nu,RC)\right] = \frac{1}{2RC} \; x \begin{cases} 0 & ; \quad z \leq 0 \\ I\left[1-\exp\left(-\frac{2z}{\nu RC}\right)\right] & ; \quad 0 \leq z \leq H \\ I\left[1-\exp\left(-\frac{2H}{\nu RC}\right)\right] \exp\left(-2\,\frac{z-H}{\nu RC}\right); & \quad z \geq H \end{cases} \tag{18}$$

Taking again z = H one has from eq. 18

$$\sigma^2(J_{max}) = \frac{1}{2RC} \cdot I \left[1-\exp\left(-\frac{2H}{\nu RC}\right)\right] \tag{19}$$

or the relative standard deviation

$$\frac{\sigma(J_{max})}{J_{max}} = \frac{1}{\sqrt{2 \cdot RC \cdot I}} \sqrt{\frac{1+\Delta}{1-\Delta}} \tag{20}$$

Where Δ is given by eq. 15 in table 1. Assuming $\Delta << 1$ one has from eq. (20) for the relative standard deviation

$$\delta = \frac{\sigma(J_{max})}{J_{max}} \tag{21}$$

that

$$RC = \frac{1}{2 \cdot I \cdot \delta^2} \tag{22}$$

In table 2 the values of RC are given according to eq. (22)

TABLE 2

The values of RC (in sec) for different error δ and intensity I values

	δ(%)				
I (cps)	1	2	5	10	20
1	5000	1250	200	50	12.5
5	1000	250	40	10	2.5
10	500	125	20	5	1.25
20	250	62.5	10	2.5	0.625
40	125	31.25	5	1.25	0.312
80	62.5	15.6	2.5	0.625	0.156
160	31.25	7.8	1.25	0.312	0.078

Once the RC value is selected, for the assumed dynamic distortion Δ, i.e. from the lag value $\nu \cdot RC$ one obtains the logging velocity ν. When one has some limited choice of the RC values for a given model of the ratemeter, one takes always the nearest higher value. For example if

$I = 5$ cps

and we want to have at least

$\delta = 5\%$

the RC from table 2 is 40. The nearest higher value of RC is for example

$RC = 80$ s

The log is recorded in the scale 1:500, i.e.

1 cm in the log = 5 m in the borehole.

One can expect that 4 mm in the log will be possible to distinguish, which means, that the H_{min} is

H_{min} = 4 mm in log = 2 m in the borehole

which for the qualitative measurement gives from eq. 16

$$0.5\ H_{min} \geq \nu RC \geq 0.33\ H_{min}$$

which is in this case

$$1\ m \geq \nu RC \geq 0.67\ m.$$

Thus for RC = 80 s one has

$$1.25\ \frac{cm}{s} \geq \nu \geq 0.8333\ \frac{cm}{s}$$

or

$$0.75\ m/min \geq \nu \geq 0.5\ m/min.$$

If for some technical reasons we have to use, for example

$\nu = 1$ m/min

it will mean that our thickness resolution (qualitatively) will be in this particular case

$$2 \cdot v \cdot RC \leq H_{min} \leq 3 \cdot v \cdot RC$$

which is in our case

$$267 \text{ cm} \leq H_{min} \leq 400 \text{ cm}$$

because

$$vRC = 1 \text{ m/min} \cdot 80 \text{ s} = 133.33 \text{ cm}.$$

When, at a given intensity (for example at a given depth in the borehole) one records the statistical variations (after the waiting time of the order of 4•RC to have the factor

$$\sqrt{\frac{1 + \Delta}{1 - \Delta}}$$

in eq. (20) close to 1), the variations observed during about 10•RC should be within the limits of $\pm 2\delta$, which means, that the recorded line for the intensity I should be

$$I - 2\sqrt{\frac{I}{2RC}} \leq I \leq I + 2\sqrt{\frac{1}{2RC}} \qquad (23)$$

which for the example given above is

$$4.64 \text{ cps} \leq I \leq 5.35 \text{ cps}.$$

When one operates in some geological region having more or less well defined and constant range of variation of geological parameters, for a given type of logging equipment, the average values of the intensities I(z) for each type of log are constant, which in turn implies always the same values of RC. When one takes the minimum lag v•RC as being equal to 100 cm, one has a very simple formula for the logging speed:

$$v = \frac{100}{RC} \frac{\text{cm}}{\text{s}} = \frac{6}{RC[s]} \frac{\text{m}}{\text{min}} \qquad (24)$$

or in general

$$\nu = c \cdot \frac{6}{RC[s]} \frac{m}{min} \qquad (24a)$$

where c is a factor of the admissible lag 100 cm (i.e. for the lag 200 cm c = 2 etc.). RC is here the ratemeter time constant (in sec) selected once for all for a given type of log (for example RC = 80 s for GR log).

2 GAMMA RAY LOG

2 GAMMA RAY LOG

J.A.C. JUNE 14, 1978

Gamma ray log is performed to measure the natural radioactivity of rocks. Sometimes artificial radioisotopes are introduced into the borehole as a tracers of liquid or solid materials. This log is then also used to locate these radioisotopes in the borehole and to measure its die-away behaviours. We will consider here only the first application, i.e. the measurement of the natural rock radioactivity. Again one distinguishes here two principal cases:

1. Application for determination of the grade of radioactive ores.
2. Application as a lithology log. We shall be interested in this latter case. In the lithology log the natural radioactivity of rocks is due to the presence of potassium (with its radioactive K-40 isotope) in the amount between 0 and 6% in igneous rocks and due to the radioactive decay of the series of uranium (mainly U-238) and thorium (Th-232) being at the level between 0 and 30 ppm, with the usual Th/U ratio of about 3. The U and Th content increases when one goes from the ultrabasic to the more acidic igneous rocks.

Finally there exist the radioactive sources in the igneous rocks, which altogether are emmiting some number of gamma photons of certain energy. The number of photons per decay is given in fig. 1 *[1]*. Each primary photon is scattered in the rock medium, undergoing usually several consecutive Compton scatterings, up to the moment when it is absorbed due to the photoelectric absorption. The simultaneous combination of these two phenomena during the photon transport through the rock media gives as a result the continuous photon energy spectrum. An example of such spectrum is given in fig. 2 *[2]*, where for the two primary photon energies E_o = 1 and E_o = 2 MeV the photon flux in photons/cm^2/sec has been calculated in function of the scattered photon energy in oxygen, silicon and iron, when each elementary volume of these media has emitted 1 photon/sec (of energy E_o). As a matter of fact in the rocks one has a superposition of such spectra due to the whole set of primary photon energies just presented in fig. 1. This combined photon spectrum is impinging with the gamma ray detector in the gamma ray tool.

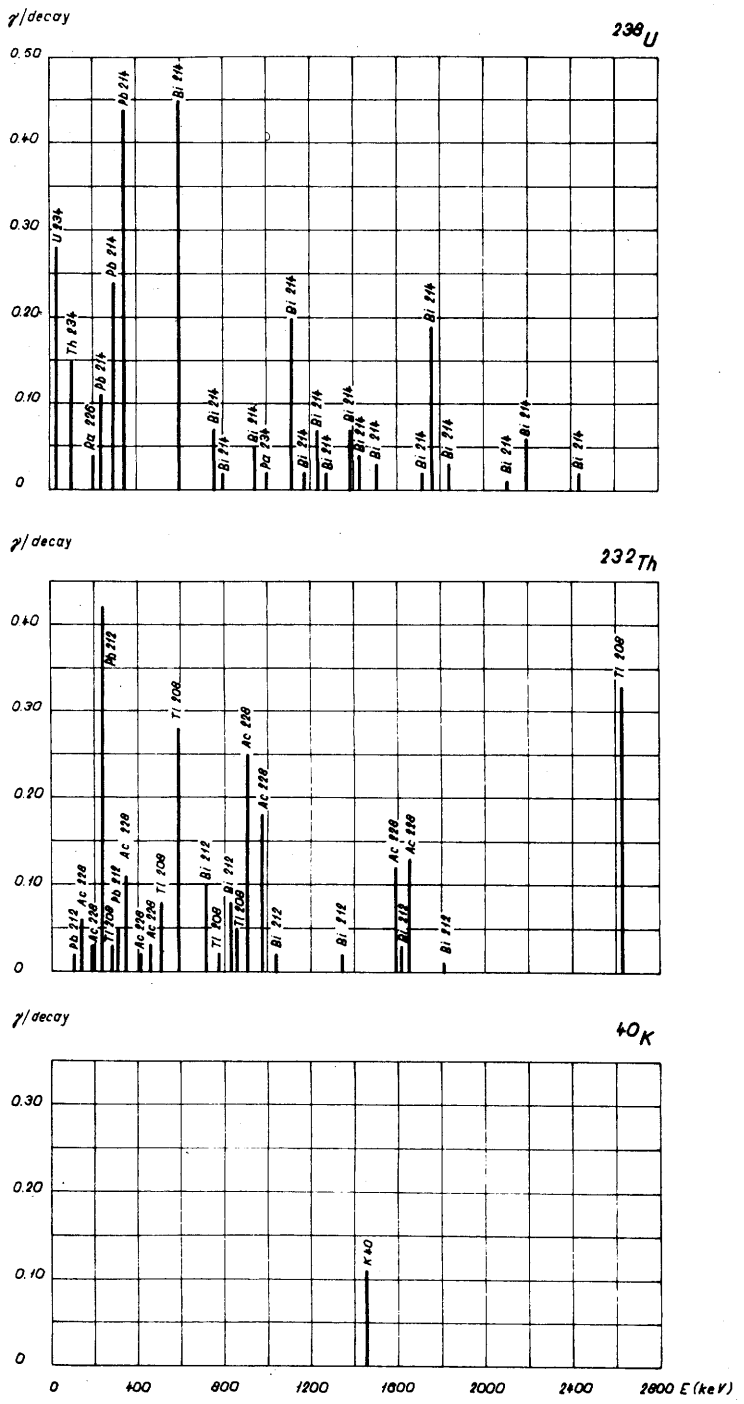

Fig. 1

Prominent gamma rays emitted by the decay products of U-238, that of Th-232 and K-40 *[1]*

The efficiency of detecting the photons of given energy is different for different detectors. As an example some of the efficiency curves of gamma detectors are given in fig. 3 *[1]*.

When the Geiger-Müller counter is used as a detector, one obtains for such combined spectrum only one figure - the total (or so called gross count) intensity. When the scintillation counter is used, the registered photon spectrum is the convolution of the physical photon spectrum with the detector response function, which gives as a result the "gamma ray spectrum", which for some probe is presented in fig. 4 (for uranium bearing rock only). In the lower part of this figure the spectrum of the radium needle measured in the air by the same probe, is shown.

As we can see from figs. 1,2 and 4, the majority of photons arriving to the detector is in the vicinity of 200 keV in spite of its initial energies (it is about 90% of photons with energies below 400 keV). This is just the region, where

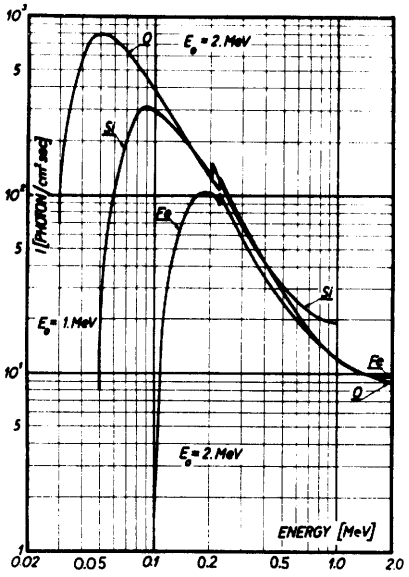

Fig. 2

Spectra of scattered γ-rays in homogeneous, infinite medium, calculated with the source strength as unity *[2]*.

the photoelectric absorption starts to be important.

Really, this effect is visible when the so called equivalent (or effective) atomic number Z_{eq} of the rock is variable in the large range. An example of such influence for rock only bearing uranium is given in fig. 5 *[1]*.

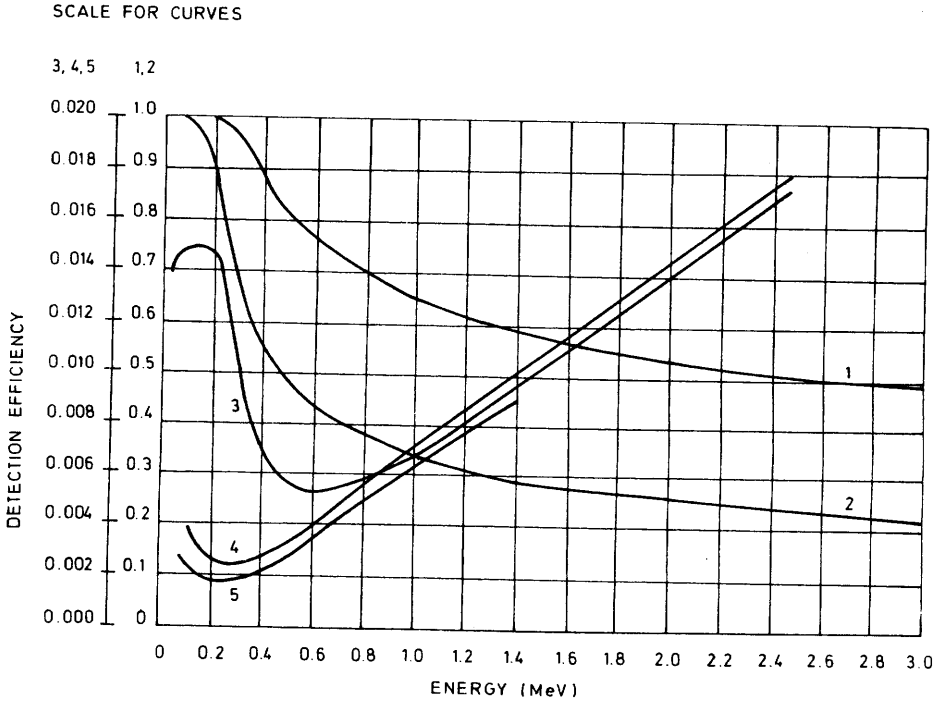

Fig. 3

Efficiency curves of gamma detectors. 1 - scintillation counter NaI(Tl), height of crystal 50 mm, 2 - scintillation counter NaI(Tl), height of crystal 20 mm, 3 - GM counter, W-cathode, 4 - GM counter, Cu-cathode, 5 - GM counter, steel cathode *[1]*

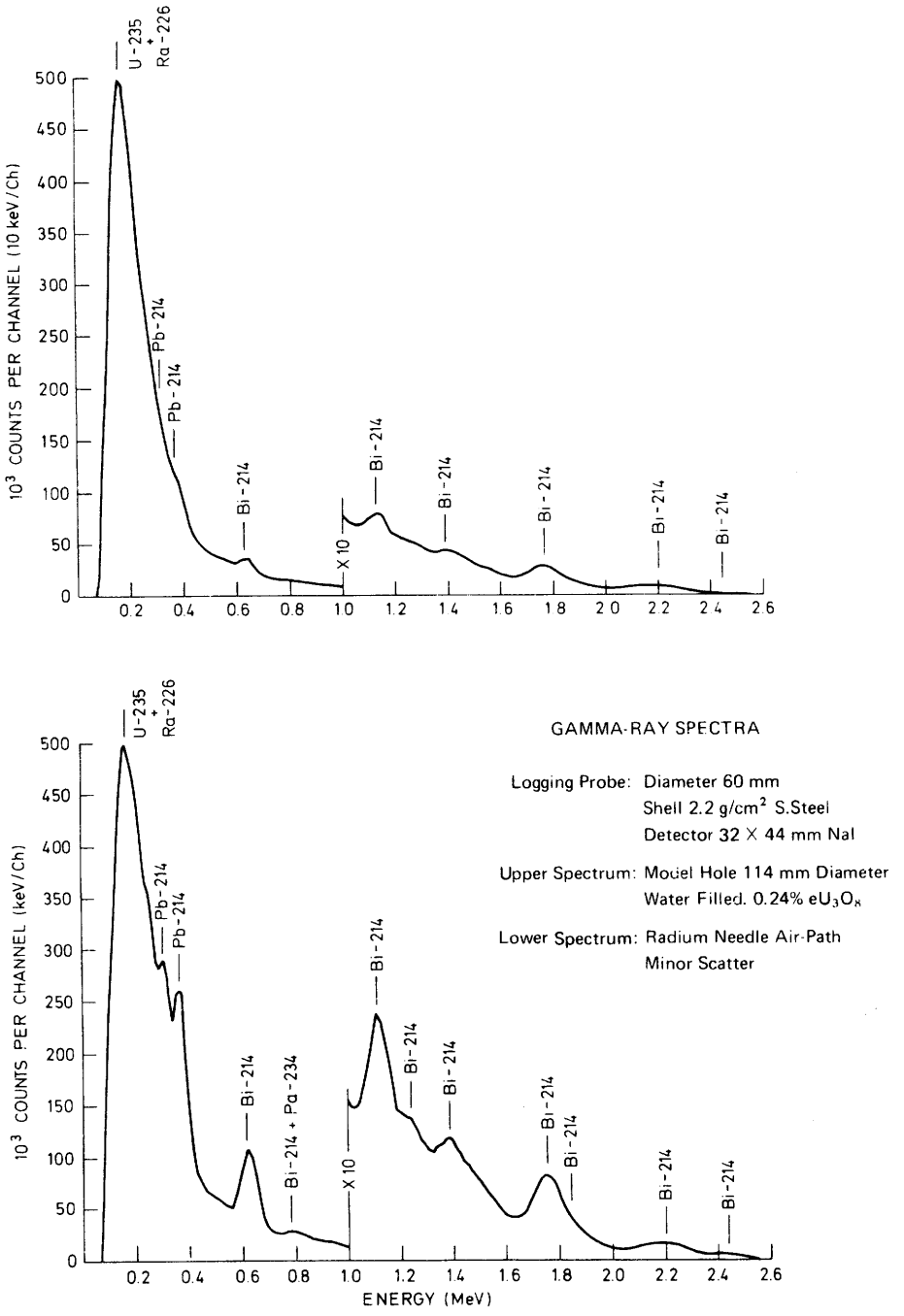

Fig. 4

Spectra measured by a typical probe show the increased fill-in and degraded resolution of primary photopeaks caused by Compton scattering in the rock and borehole environment *[1]*

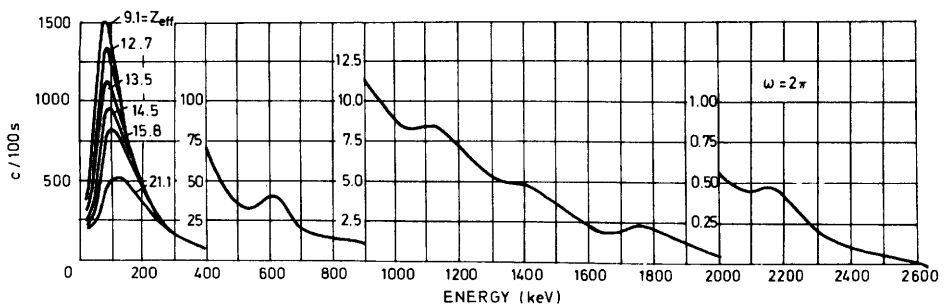

Fig. 5

Gamma spectra of uranium ores of different compositions (semi-infinite space *[2]*) *[1]*

2.1 Simple theoretical approach

In the gamma-ray log (of the lithology type) the information sought is the determination of the type of lithology and its localization along the borehole depth (its position and thickness).

The lithology is characterized by its specific radioactivity, which as a matter of fact is not a very well defined quantity. It is usually expressed in uranium equivalent ppm (or radium equivalents), which simply means that given type of rock when measured using any particular γ-ray detector (or gamma ray logging tool) gives in the same measurement condition the same signal (count rate) as the rock containing a given amount (in ppm or per cent) uranium being in the secular equilibrium with its decay products. This more or less ambiguous definition is in some countries used in the more precise way by defining the detector signal in the exposure dose units (i.e. in micro-roentgens per hour - μR/h *[3]*). This unit, however, connected more or less with the radiation field in the air (and with the spectral response of the detector tool) has some not very well defined relation to the real specific activity of the rock, which should be expressed as some weighted average (over all radioactive isotopes existed in the rock) of the Ci/g (curie per gram of rock) *[3]*.

The most adequate units of measurement for the lithology gamma ray log are the so called API γ-ray units. They are defined by means of some standard radioactive media containing about 24 ppm Th, 12 ppm U and 4% K (U and Th being in radioactive equilibrium) which, roughly speaking, corresponds to the twice of the specific radioactivity of the mid-continental shale in USA. This facility is situated at the University of Houston (Texas), and its simplified sketch is given in fig. 6. The difference in the counting rate of a given logging tool between the radioactive concrete and the low activity concrete in this facility has been defined as 200 API γ-ray units (note that there is 5 1/2" water filled and cased borehole inside), the radioactivity of the most common sedimentary rocks in the API units is given in fig. 7 *[4]*. These data are in some way recalculated from the work of Russel published in Geophysics in 1944.

Whatever unit of the specific radioactivity of rock is used, it can be characterized by its amount q. In this case, one assumes the infinite, homogeneous medium with the specific radioactivity equal q, the count rate

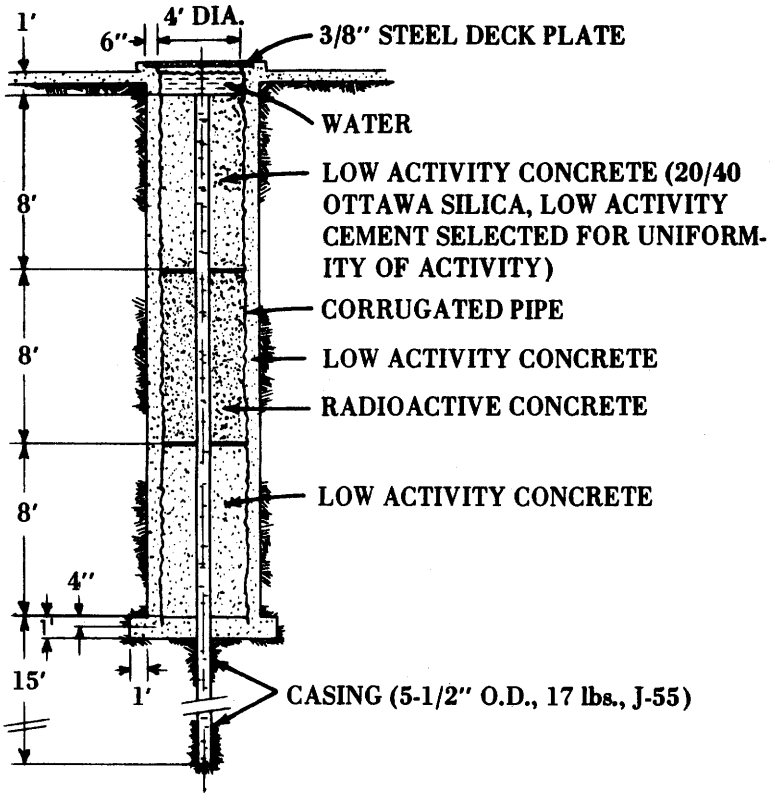

Fig. 6 *[4]*

API gamma ray calibration pit

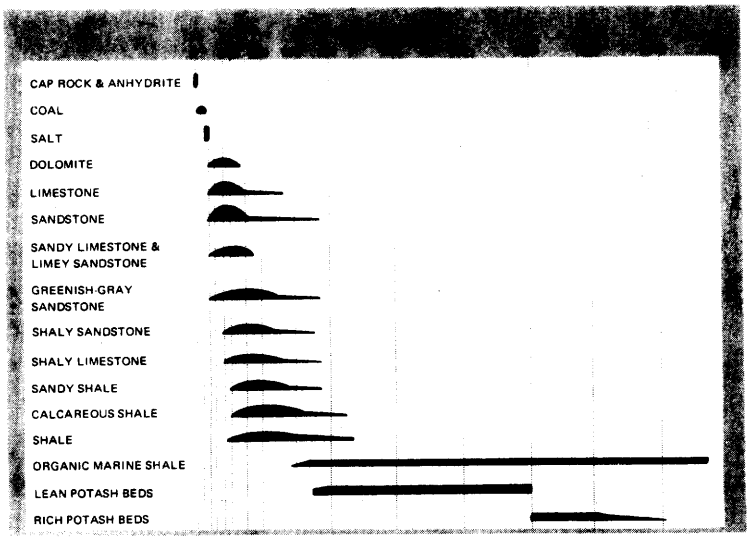

Fig. 7 *[4]*

The level of radiation normally associated with various rock types.
The length of the line denotes the intensity range in API Gamma Ray Units.
The vertical width of the line increases with the frequency of occurrence

registered by a given probe, say I_∞, is:

$$I_\infty = K \cdot q \qquad (1)$$

where K is the calibration factor depending upon the tool properties (rock properties) and upon the kind of unit used for the q determination. In any case q is here always given in the amount of radioactive material per unit weight of the natural radioactive medium (it means together with water existing in the porous space, for example), thus we call q the wet weight content, or the in situ weight content. The majority of the rock properties (for Z_{eq} constant) is in the "fine structure" of the calibration factor K, which in turn can be rewritten as:

$$K = K^1 \cdot \frac{\rho}{\mu} \qquad (2)$$

Where K^1 is the new calibration factor, ρ is the bulk density of the rock (together with its porous space water) and μ is the effective linear absorption coefficient for the registered radiation. In fact, the quantity $\frac{\mu}{\rho}$ having the meaning of the mass absorption coefficient does not depend upon the rock density (nor K^1 does). In this respect eq. (1) is density independent when q is the weight content.

Eq. (1) is valid in the infinite, homogeneous medium and also when this rock medium is crossed by the dry borehole (cf. fig. 8).

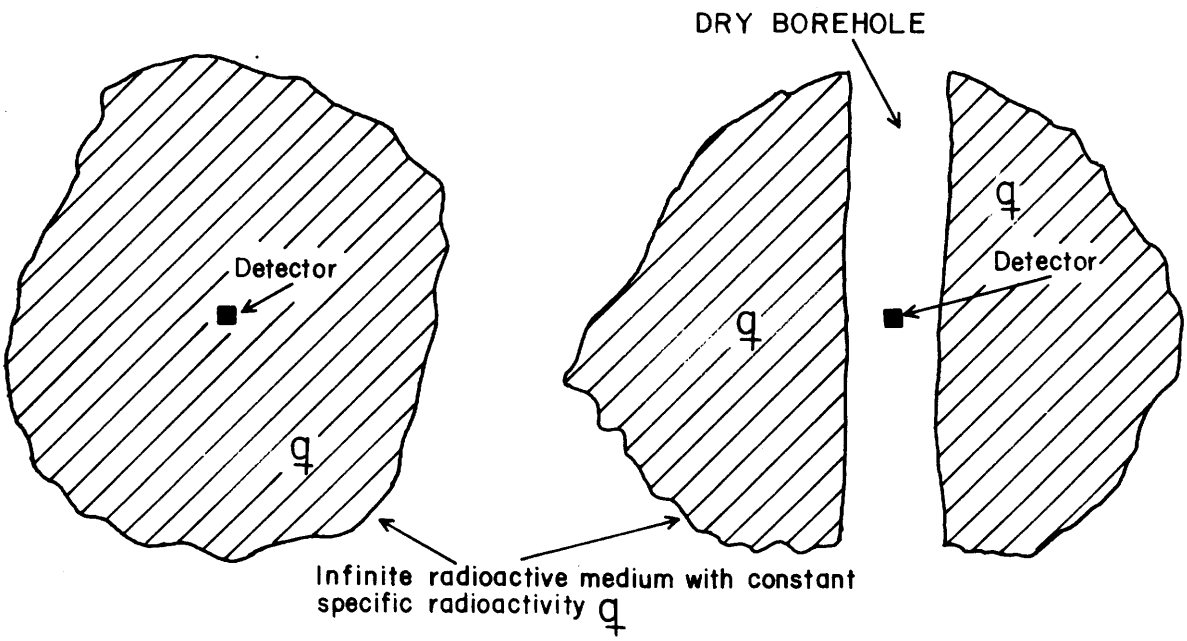

Fig. 8

Cases to which eq. (1) can be applied

When the borehole is filled with water or drilling fluid, the recorded intensity, say I_1, should be corrected by a factor CF, in order to obtain the true intensity I_∞, i.e.

$$I_\infty = CF \cdot I_1 \tag{3}$$

The correction factor CF depends upon several variables:

R - radius of the borehole

R_s - radius of the probe

ρ - density of the drilling fluid or

μ_p - effective mass absorption coefficient for the drilling fluid, which in the case of the natural radioactivity of rock is taken as

$$\mu_p \approx 0.03 \cdot \rho \tag{4}$$

ε - off-axial position of the tool in the borehole (ε=0 for central position, ε=1 for the tool completely decentralized).

The values of the so called borehole absorption function $A_p(\mu_p R)$ related to the CF correction factor by

$$CF = \frac{1}{1 - A_p(\mu_p R)} \tag{5}$$

are given in fig. 9 *[5]* for the case when the tool is completely decentralized. For the 1 11/16" GR tool of GOI the graphs of the CF correction factors can be found on pp. 176 and 178 of the GOI formation evaluation data handbook (Fort Worth, Oct. 1975).

When the radioactive formation is not infinite in the vertical direction (say, along the z-axis) the I_1 intensities are no more z independent. Some simple theoretical approach *[6]* permits to obtain in this case the shapes of the radioactive anomalies observed in this case. The main features of such anomalies for the regular radioactive layers have been calculated according to this theory *[7]*. The general behaviour is that for the semi-infinite radioactive layer the gamma ray anomaly in the vicinity of its boundary (i.e. at about 0.5 to 1.0 meter from it) has the shape

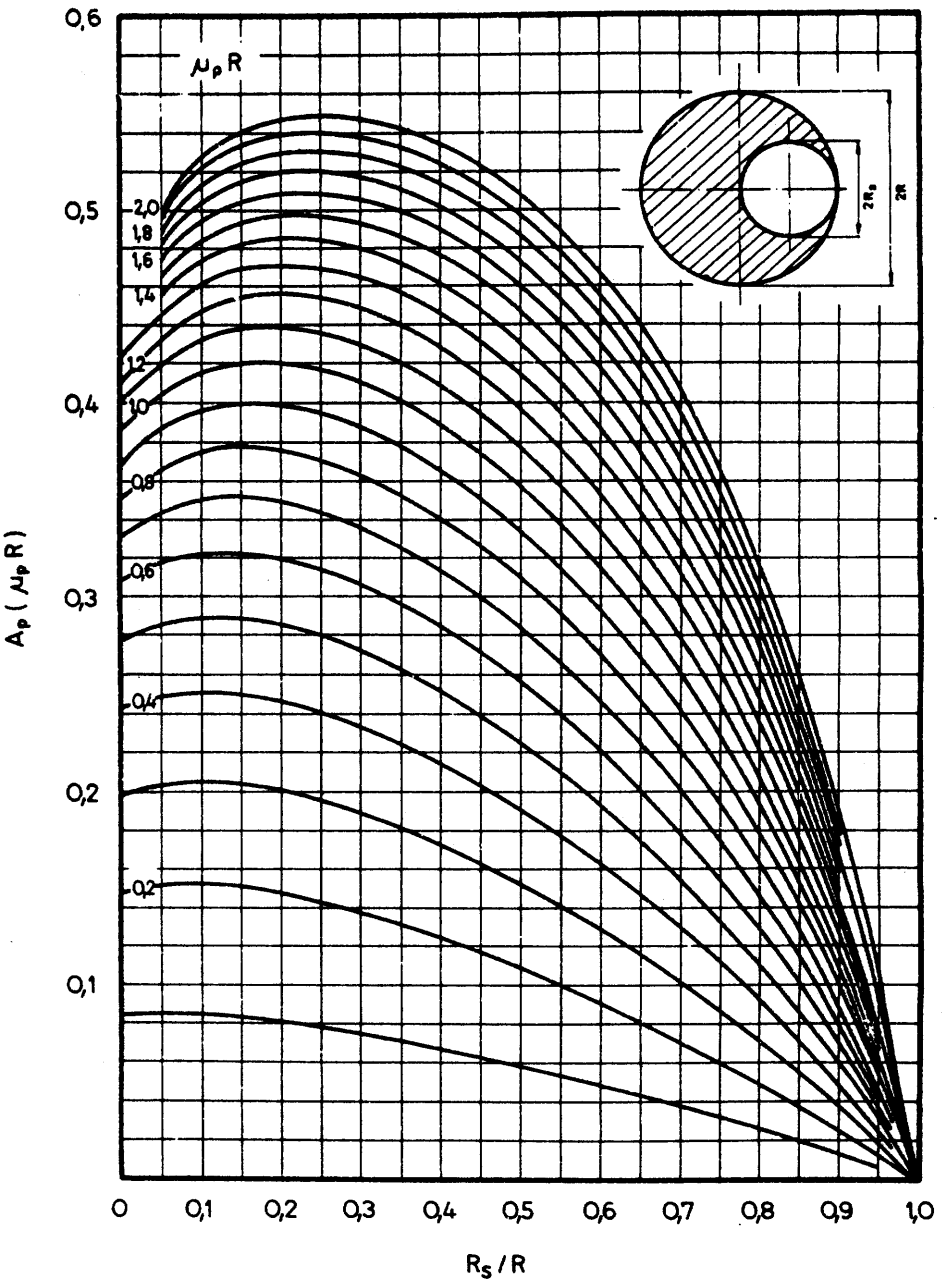

Fig. 9

Absorption function $A_p(\mu_p R)$ of the borehole fluid

R - borehole radius

R_s - probe radius

$\mu_p = 0.03 \cdot \rho$

ρ - fluid density

$$F(z) = \frac{I_1(z)}{I_\infty} \cdot CF \qquad (6)$$

given in fig. 10. The half value of this anomaly occurs exactly at the point z where the boundary is crossing the borehole. When the borehole radius R increases the slope of the anomaly F(z) decreases as shown in fig. 11.

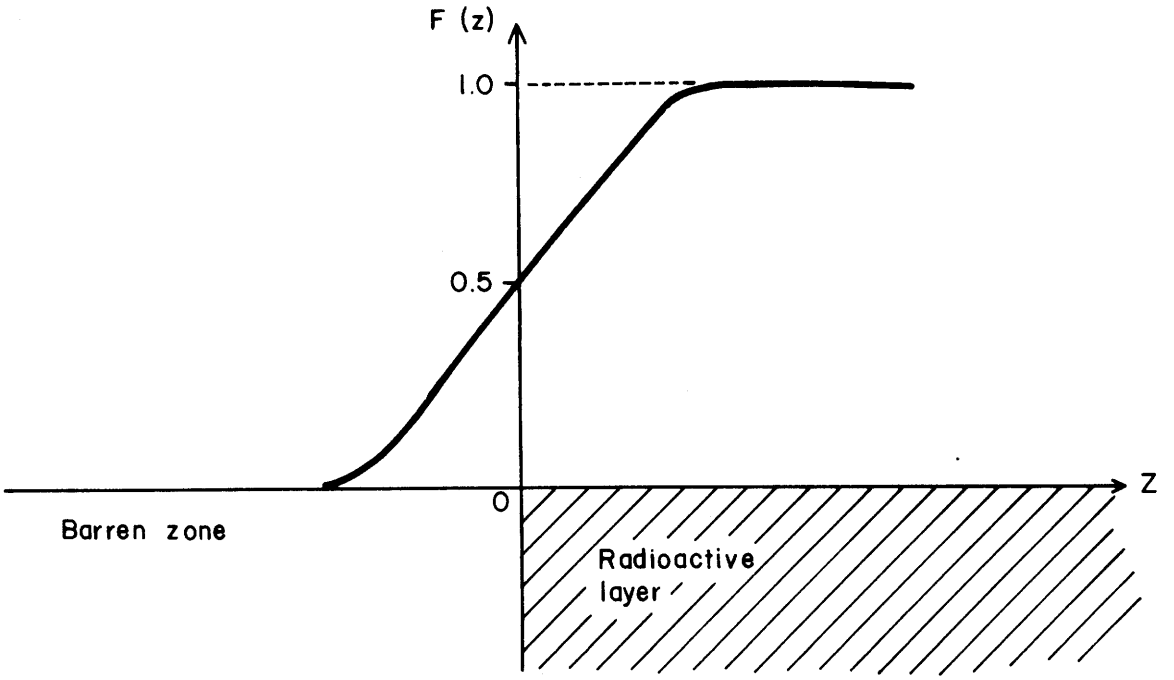

Fig. 10

Behaviour of the anomaly from the semi-infinite radioactive layer.

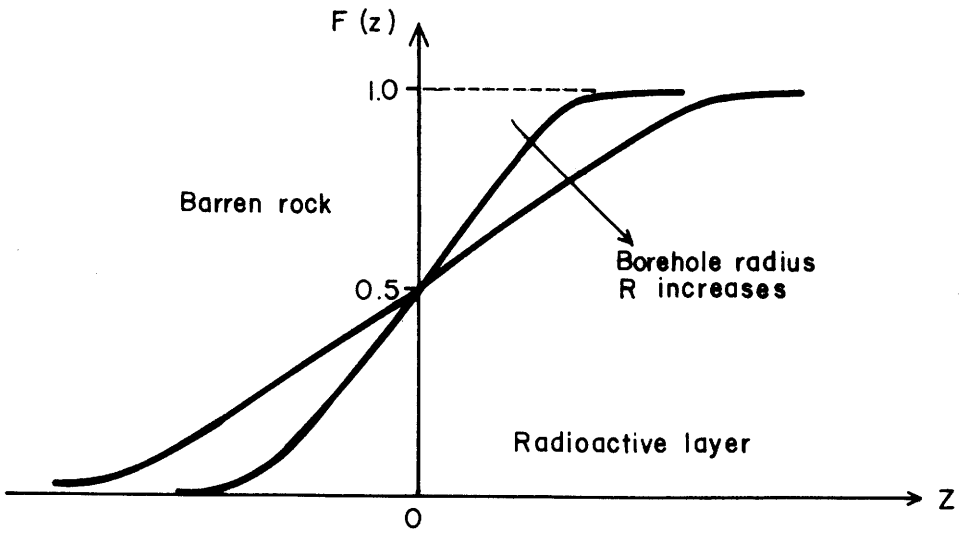

Fig. 11

Influence of the borehole radius R on the shape of the semi-infinite anomaly F(z)

When one considers the influence of the detector length L on the shape of the semi-infinite anomaly, when $F_o(z)$ denotes this shape for L = O (point-like detector), the relation is:

$$F_L(z) = \frac{1}{L} \int_{z - \frac{L}{2}}^{z + \frac{L}{2}} F_o(z^1)\, dz^1 \qquad (7)$$

which gives, of course the picture (fig. 12):

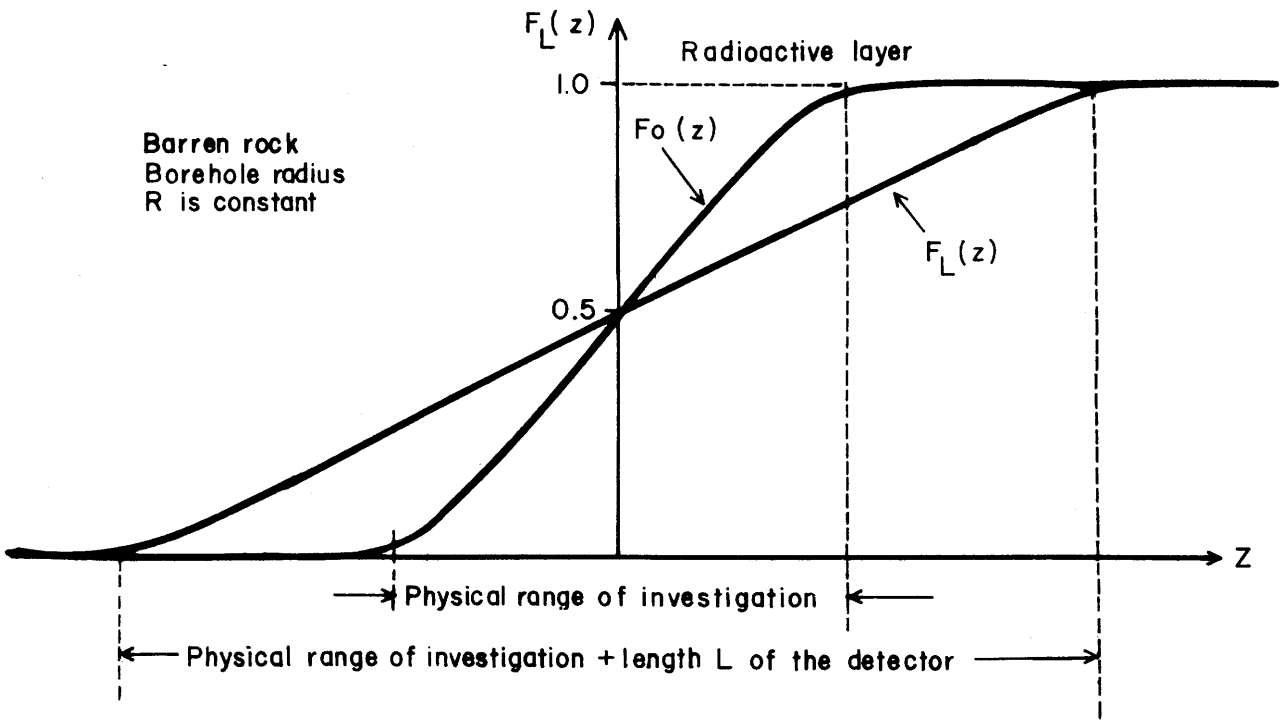

Fig. 12

Influence of the detector length L on the shape of the semi-infinite anomaly

Now, when one wants to know, what is the shape $\phi_{O,O}(z)$ of the gamma ray anomaly from the infinitely thin (thickness H → O) radioactive layer imbedded in the barren rock (cf. fig. 13).

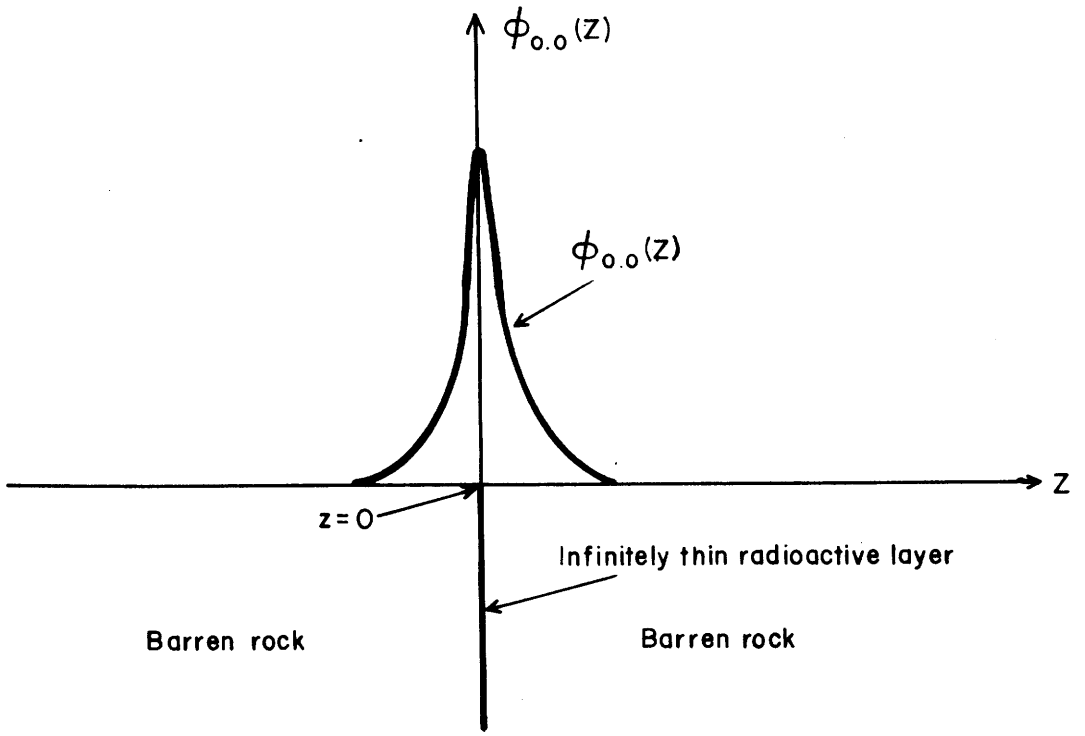

Fig. 13

Shape $\phi_{O,O}$ (z) of the GR anomaly from the layer with thickness $H \to 0$

the formula is valid

$$\phi_{O,O}(z) = \frac{d\, F_o(z)}{dz} \tag{8}$$

where $F_o(z)$ is shown in fig. 12. Now, when the thickness H is finite, the shape $\phi_{O,H}$ (z) of GR anomaly will be the superposition of the $\phi_{O,O}$ (z) anomalies, i.e.

$$\phi_{O,H}(z) = \frac{1}{H} \int_{z - H/2}^{z + H/2} \phi_{O.O}(z^1)\, dz^1 \tag{9}$$

which can easily be converted using eq. (8) to the form:

$$\phi_{O,H}(z) = F_o\left(z + \frac{H}{2}\right) - F_o\left(z - \frac{H}{2}\right) \tag{10}$$

For the tool with the finite length L of the detector the similar equations hold:

$$\phi_{L;O}(z) = \frac{d\,F_L(z)}{dz} \tag{11}$$

$$\phi_{L;H}(z) = \frac{1}{H} \int_{z-\frac{H}{2}}^{z+H/s} \phi_{L,O}(z^1)\,dz^1 = \tag{12a}$$

$$= F_L\left(z+\frac{H}{2}\right) - F_L\left(z-\frac{H}{2}\right) = \tag{12b}$$

$$= \frac{1}{L} \int_{z-\frac{L}{2}}^{z+\frac{L}{2}} \phi_{O,H}(z^1)\,dz^1 = \tag{12c}$$

$$= \frac{1}{L} \int_{z-\frac{L}{2}}^{z+\frac{L}{2}} \left[F_O\left(z^1+\frac{H}{2}\right) - F_O\left(z^1-\frac{H}{2}\right)\right] dz^1 \tag{12d}$$

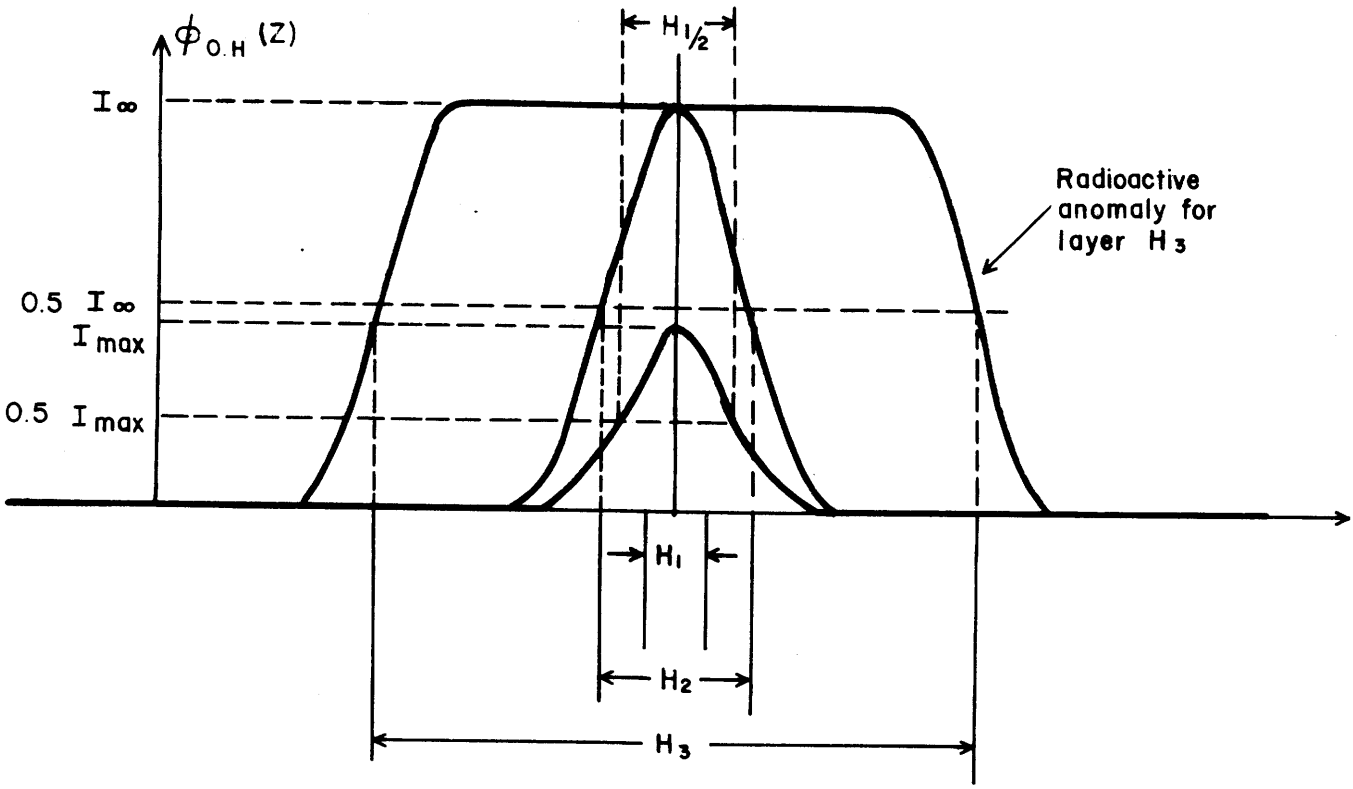

Fig. 14

Influence of the layer thickness on the shape of radioactive anomaly

The thickness H of the radioactive layer has an important influence on the shape of the GR anomaly. This influence, for L = 0, according to eq. (10) can be illustrated by a simple sketch given in fig. 14. Here the three layers with thickness $H_3 > H_2 > H_1$ give three radioactive anomalies characterized by following features:

Layer with thickness H_3 has a flat maximum equal to I_∞ because H_3 value is much greater than the range of investigation (which is of order of about 1 meter) of the method. In this case the value of anomaly at its half maximum ($0.5\ I_\infty$) indicates the position of the true boundary of the radioactive layer.

When the thickness H_2 is just equal to the range of investigation, the radioactive anomaly has still the maximum equal to I_∞ which is now no more flat but is a real peak. Its half maximum thickness $H_{1/2}$ indicates the real boundaries of the radioactive layer.

Finally, when the thickness H_1 is much smaller than the range of investigation, the maximum value I_{max} of such anomaly is:

$$I_{max} \leq I_\infty$$

and consequently

$$H_{1/2} \geq H$$

When one compares eq. (9) with eq. (12c) one easily finds that the effect of the detector length L is manifested with the same way as the effect of the layer thickness H. For this reason the maximum space resolution (in the z-axis direction) for the gamma-ray method is equal at least to the length L of the detector used for the gamma-ray log.

All these effects enumerated above give the behaviour of the main parameters I_{max} and $H_{1/2}$ of the gamma ray anomaly, of a single radioactive layer with thickness H crossed by the borehole with radius R, and when the anomaly is measured with the detector of the length L, which is schematically presented in figs. 15, 16, 17 and 18.

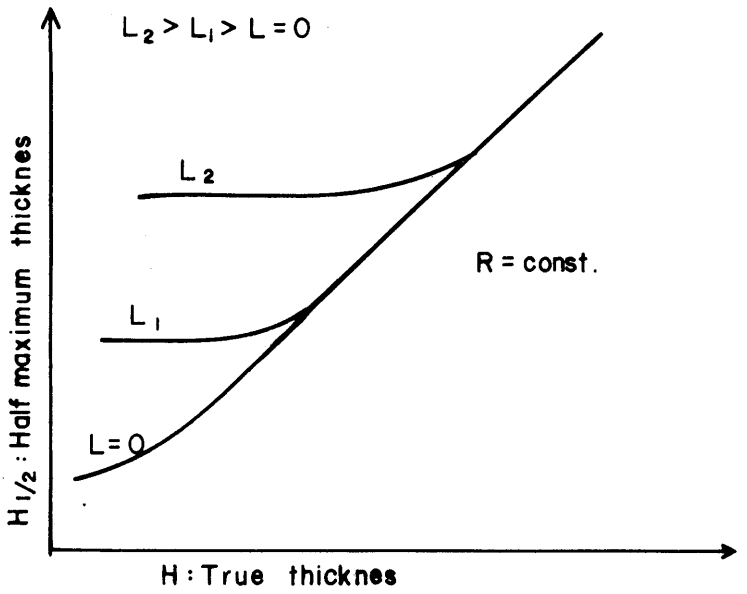
$L_2 > L_1 > L = 0$
L_2
R = const.
L_1
L=0
$H_{1/2}$: Half maximum thicknes
H : True thicknes

Fig. 15

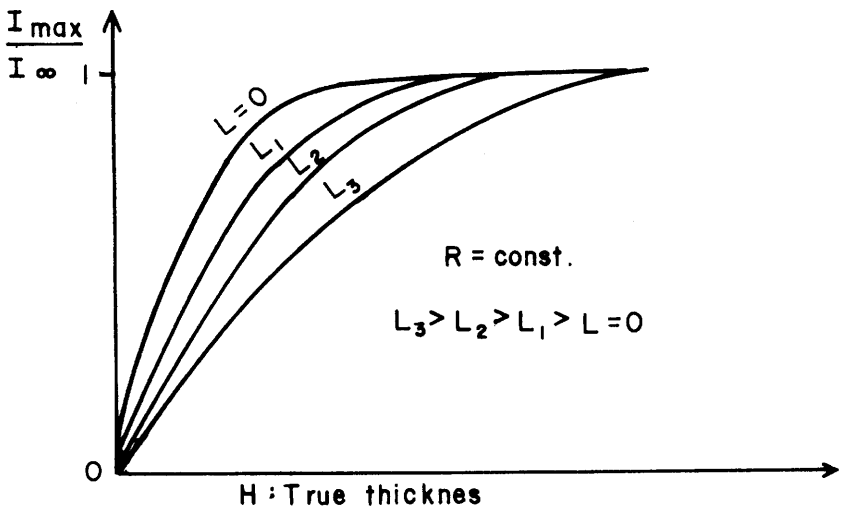
$\frac{I_{max}}{I_\infty}$
1
L=0
L_1
L_2
L_3
R = const.
$L_3 > L_2 > L_1 > L = 0$
0
H : True thicknes

Fig. 16

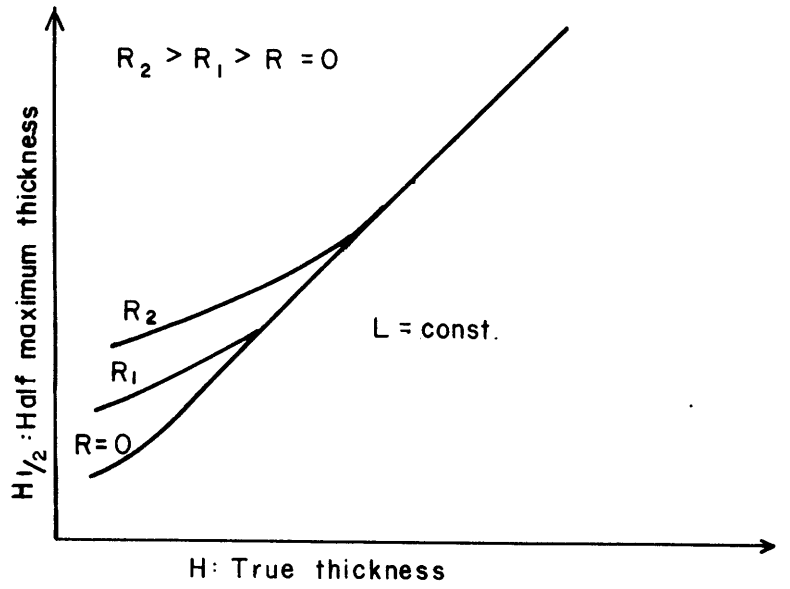
$R_2 > R_1 > R = 0$
$H_{1/2}$: Half maximum thickness
R_2
R_1
R=0
L = const.
H: True thickness

Fig. 17

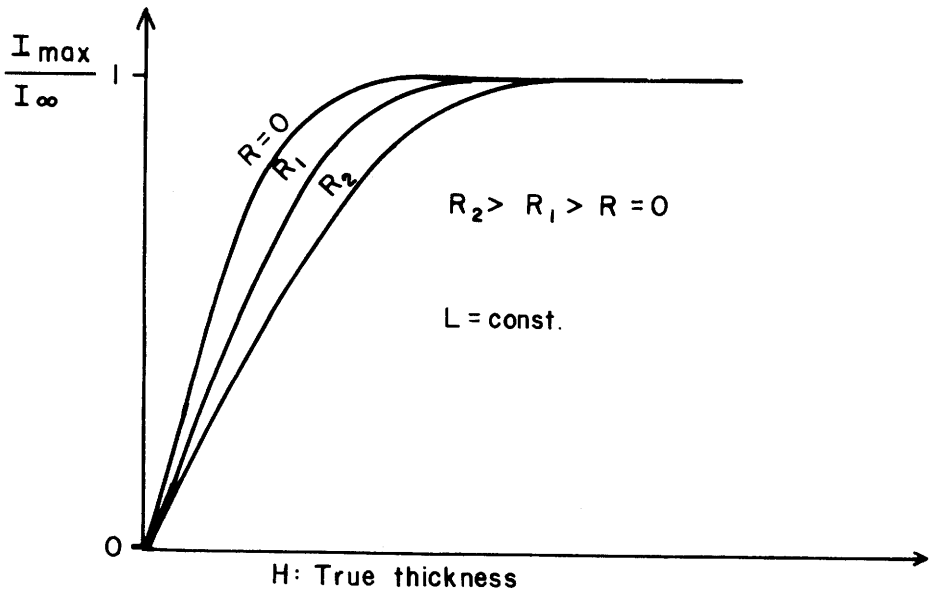
$\frac{I_{max}}{I_\infty}$
1
0
R=0
R_1
R_2
$R_2 > R_1 > R = 0$
L = const.
H: True thickness

Fig. 18

When one takes, however, the total area under the radioactive anomaly, i.e.

$$S = \int_{-\infty}^{+\infty} I(z)\, dz \tag{13}$$

one obtains that

$$S \cdot CF = I_{\infty} \cdot H = K \cdot H \cdot q, \tag{14}$$

where CF is given in eq. 3. This last relation (so called GT: Grade x Thickness) is used in USA to obtain the calibration factor from the area S of the known anomaly of the uranium bearing layer (but attention! they define their calibration factor as being equal to $\frac{1}{K \cdot H}$ according to the symbols used here!).

In the lithology log we are interested in the knowledge of I_{∞}, not q, to be able to compare different layers. The I_{∞} value can be given either in cps (when one has only one logging equipment) or in the API gamma ray units. The procedure, how to get I_{∞} from measurement, being the inverse way of application of eq. 14 or nomograms in figs. 15÷18 is called the interpretation and is usually performed using the computers and following one of the particular theories of interpretation of the gamma ray logs.

2.2 Introduction to the theory of interpretation of gamma ray logs

Modern methods of interpretation of gamma ray logs are not taking into account only one separate radioactive layer but their whole sequence in the borehole. Here the assumption is that the layers are parallel and the borehole is perpendicular to them. In this case the registered signal $I_1(z)$ at a given depth z is equal to:

$$I_1(z) = K \cdot \int_{-\infty}^{+\infty} \frac{1}{CF(z^1)} \cdot q(z^1) \cdot \phi_{L,O}\,(|z-z^1|)\, dz^1 \approx \tag{15a}$$

$$\approx \frac{1}{CF(z)} \int_{-\infty}^{+\infty} I_{\infty}(z^1) \cdot \phi_{L,O}\,(|z-z^1|)\, dz^1 \tag{15b}$$

The sense of eq. 15 is that the registered anomaly $I_1(z)$ is a superposition of many elementary anomalies $\phi_{L,O}(z^1)$ having each its center at the point z^1.

When one extends these infinitely thin elementary layers to the finite thickness Δh, we shall have the situation presented in fig. 19 *[9]* . The whole theory of interpretation is explained in the papers *[8, 9, 10, 11]* and here we shall give short description of this method of interpretation.

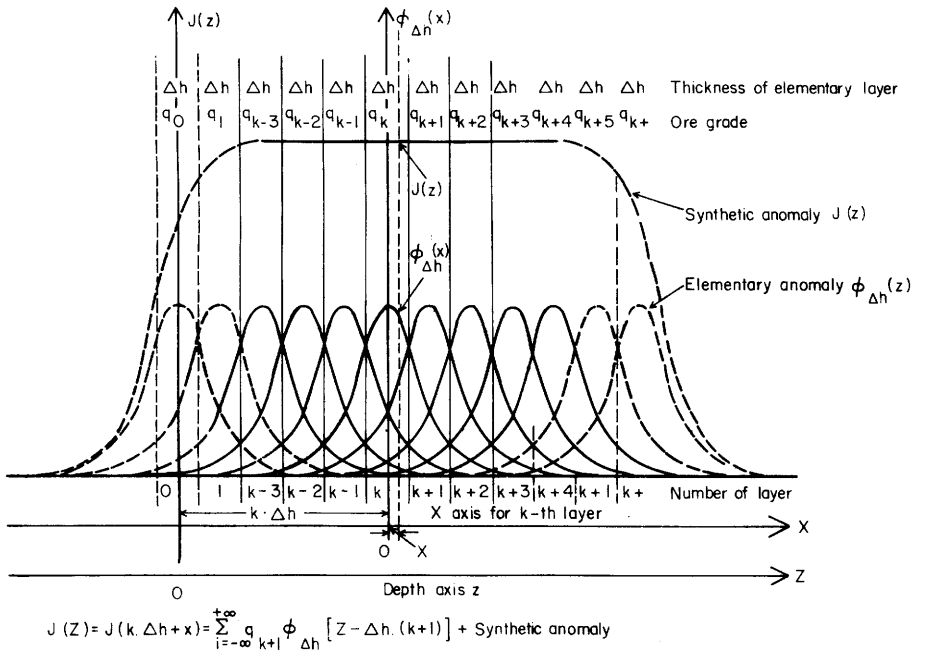

Fig. 19 *[9]*

The principle of the synthetic anomaly J(z) composed from the elementary anomalies $\rho_{\Delta h}(X)$, for which all q_h are equal and constant

First, one digitalizes the analog record of the dynamic curve taking its digitalized values $J(z_k)$ in the middle of each elementary layer of thickness Δh, just as it is shown in fig. 20. The static gamma ray curve $I(z_k)$ is obtained using the algorithm:

$$I(z_k) = \sum_{j=-p}^{+p} J(z_{k+j}) \cdot g_j(p) \qquad (16)$$

where for

$$j \neq 0$$

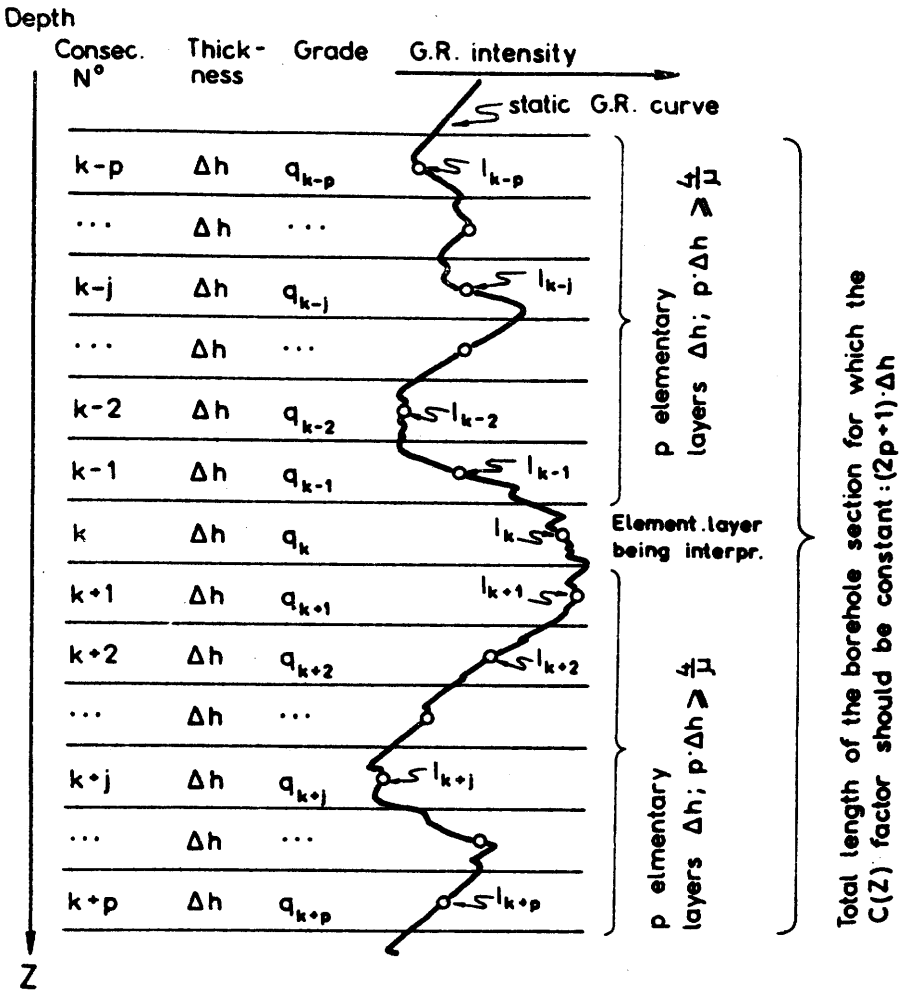

Fig. 20 *[8]*

Mutual positions of gamma ray intensities I_i and ore grades q_i taken into account in the interpretation procedure

$$g_j(p) = - g_{-j}(p) = - \frac{\nu \cdot RC}{\Delta h} (-1)^j \frac{p!\ p!}{j \cdot (p+j)!\ (p-j)!} \tag{17}$$

and for $j = 0$

$$g_o(p) = 1 \tag{18}$$

The values $-p \leq j \leq +p$ increase along the direction of the logging speed ν. Each static value $I(z_k)$ is corrected, if necessary, to the detector dead time τ loss:

$$I_1(z_k) = \frac{I(z_k)}{1 - \tau \cdot I(z_k)} \tag{19}$$

Next each $I_1(z_k)$ value is corrected to the different radiation absorption in the drilling fluid due to the variation in borehole diameter 2R:

$$I^{o}(z_k) = I_1(z_k) \cdot CF(z_k,R) \tag{20}$$

Finally the $I_\infty(z_k)$ value is calculated from the formula:

$$I_\infty(z_k) = \sum_{j=-p}^{j=+p} I^{o}(z_k) \cdot b_j(p) \tag{21}$$

which is nothing else but the solution of the integral equation (15b). The $b_j(p)$ coefficients are:

$$b_j(p) = b_{-j}(p) =$$

$$= \delta_{oj} + A_j(p) + \frac{B_j(p)}{\alpha^2 \cdot \Delta h^2} \tag{22}$$

Here δ_{oj} is the Kronecker's delta:

$$\delta_{oj} = \begin{cases} 1 & \text{for } j = 0 \\ 0 & \text{for } j \neq 0 \end{cases} \tag{23}$$

and in ref. 8 there are the extensive tables of the coefficients $A_j(p)$, $B_j(p)$ and α.

How this kind of interpretation "works" can be seen in figs. 21 and 22. For the GR anomaly N° 1 in fig. 21 its digitalized values have been taken (curve N° 1 in fig. 22). Next the values of $I^{o}(z_k)$ (Δ) and $I_\infty(z_k)$ are shown in fig. 22.

Example

As an example we can take the question, how to restore the static anomaly I(z) from the registered J(z) dynamic one. Let us take the worst conditions, when the static anomaly has the rectangular shape. Let its thickness be H = 5 m, the $v \cdot RC$ is $v \cdot RC$ = 1 m/min · 80 sec = 133.333 cm. In this

case the $I(z)$ values are given for $I(z)$:

$$I(z) = \begin{cases} B & z \leq 0 \\ B + I & 0 \leq z \leq H \\ B & z \geq H \end{cases}, \tag{24}$$

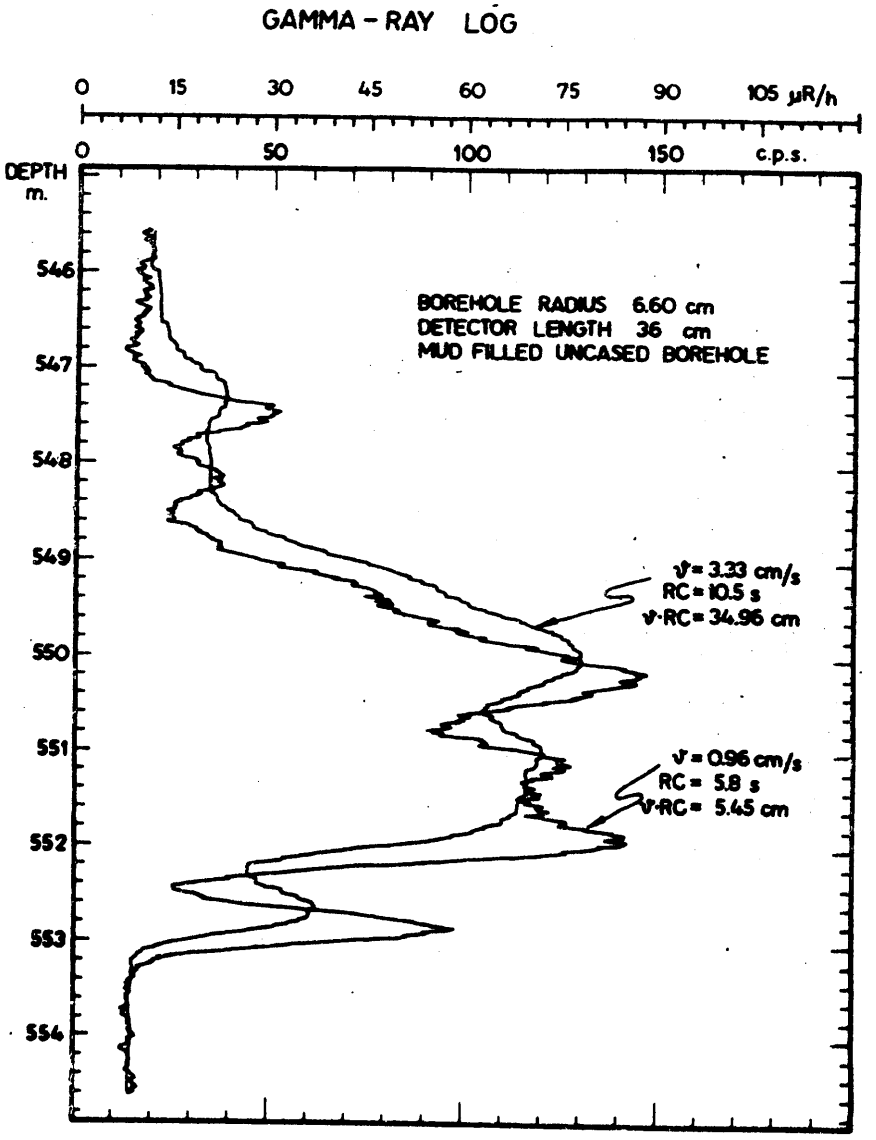

Fig. 21 *[8]*

Influence of the logging speed ν and the ratemeter time constant RC on the shape of the dynamic anomaly $J(z)$

where B in eq. (24) can be considered as a constant background. The dynamic anomaly is given, according to eq. (1.6) or (1.13) as:

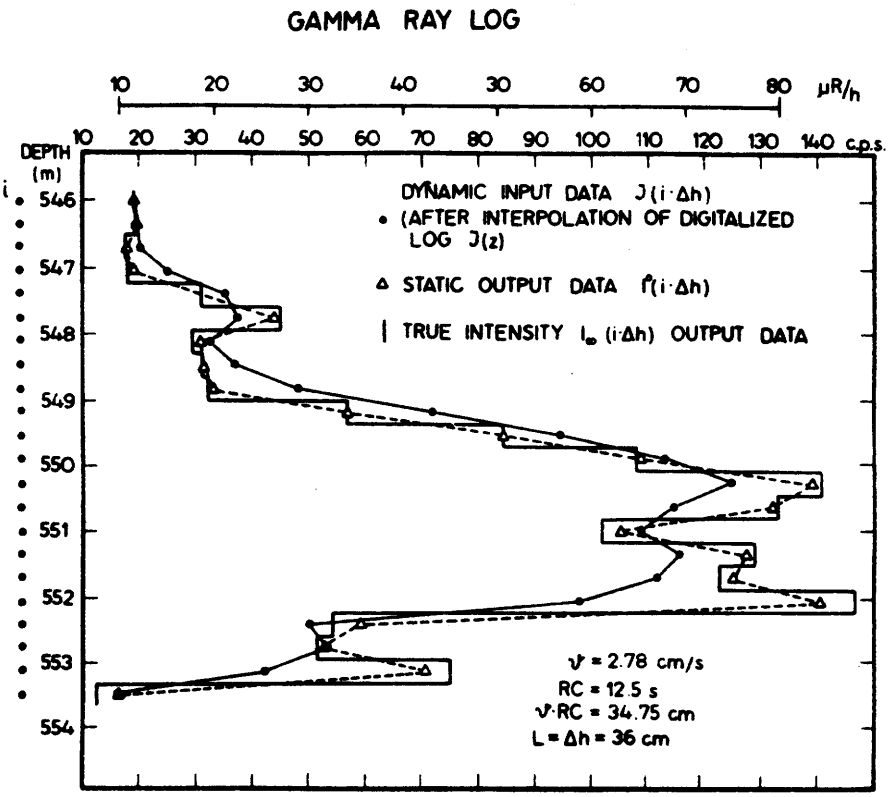

Fig. 22 *[8]*

Example of the gamma ray log interpretation on uranium deposit. Uncased borehole, diameter 132 mm. Linear absorption coeff. taken for interpretation: $\mu = 0.09\ cm^{-1}$, $p = 4$

$$J(z) = \begin{cases} B & 0 \geq z \\ B + I\,(1 - e^{-\frac{z}{133.333}}) & 0 \leq z \leq H \\ B + I\,(e^{\frac{500}{133.3}} - 1) \cdot e^{-\frac{z}{133.333}} & z \geq H \end{cases} \qquad (25)$$

We take the values of the above J(z) function at the points

$$z_k = k \cdot \Delta h = k \cdot 45.72\ cm \qquad (26)$$

$$k = 0, 1, 2, 3 \ldots\ldots$$

which corresponds to the digitalization of the analog record J(z) of the log.

Now, to restore again the $I(z_k)$ we use eq. (16) for p = 3 (which gives $p \cdot \Delta h$ = 137.16 cm which is bigger than the range of investigation). The $g_j(3)$ values calculated from eq. (17) are in this case:

$$g_o(3) = 1.0000$$
$$g_1(3) = -g_{-1}(3) = 2.1872$$
$$g_2(3) = -g_{-2}(3) = -0.4374$$
$$g_3(3) = -g_{-3}(3) = 0.0486$$

and the formula (16) becomes:

$$I(z_k) = J(z_k) + 2.1872 \times [J(z_{k+1}) - J(z_{k-1})] -$$
$$- 0.4374 \times [J(z_{k+2}) - J(z_{k-2})] + 0.0486 \times [J\ z_{k+3}) - J(z_{k-3})]$$

The application of this formula gives the result which is presented in fig. 23. As we can see the restored $I(z_k)$ values do not follow perfectly the input I(z) static anomaly, especially near the boundaries. This effect is due to the rectangular shape of the static anomaly. If it is more smooth (which is the case in the nature) these deviations at the boundaries become negligible.

As an exercise the reader can repeat this example but taking $v \cdot RC$ = 400 cm (i.e. 3 times higher than in the example). In practice this vRC value should be achieved not by increasing the RC value (which can be not available for a given ratemeter module) but by increasing by the factor 3 the logging velocity. This conserves the same accuracy of measurement (cf. eq. 1.11) but increases the dynamic distortion (cf. eq. 1.15). The main task of the procedure prescribed by eq. 16 is just to restore the right values of I(z) from such very distorted recorded log values. This simply means that application of eq. 16 permits to save time doing the log run quicker.

Some more details on the application of digital method of interpretation, given above, can be found in ref. 12.

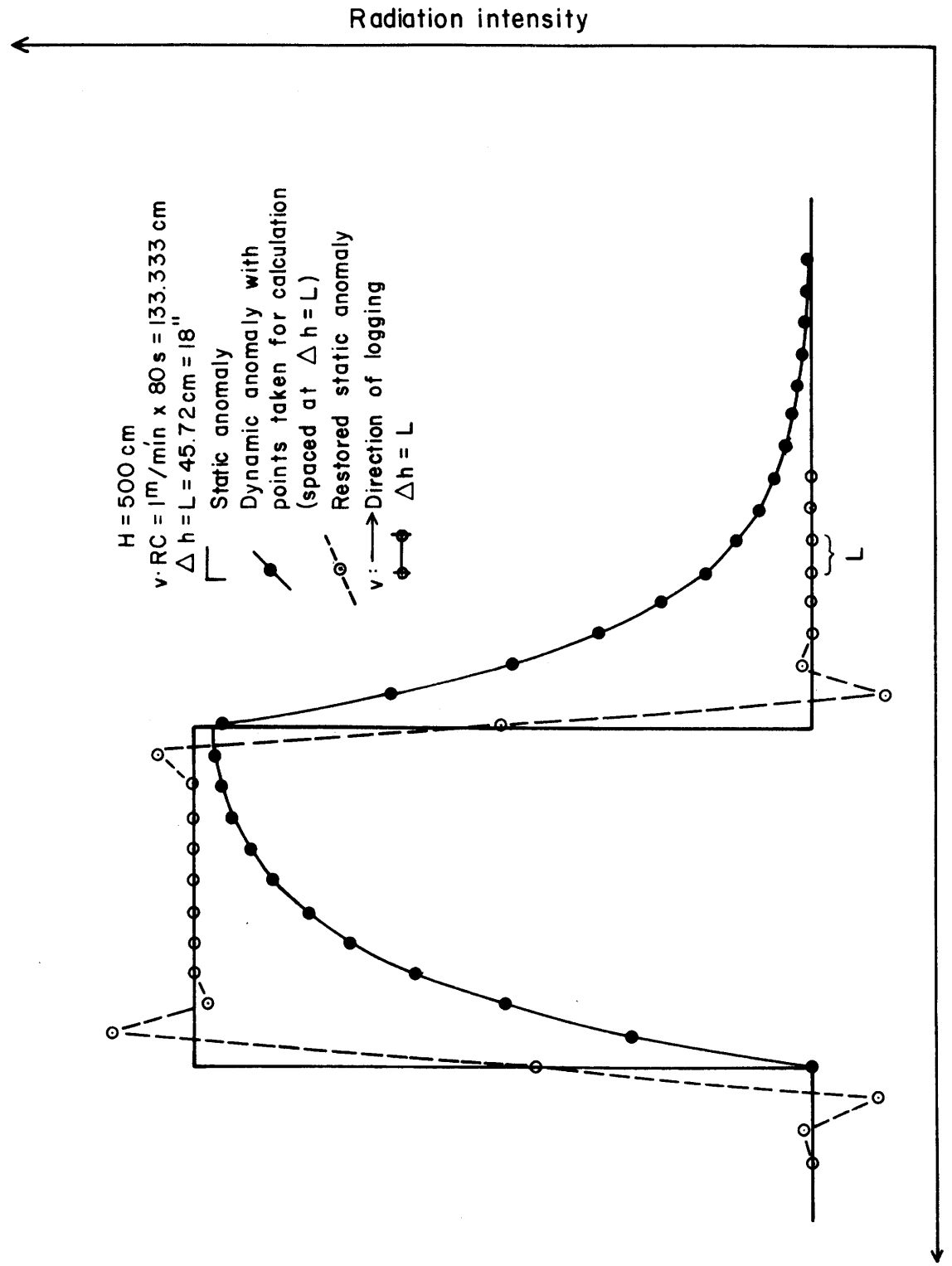

Fig. 23

Graphic presentation of the example for application of eq. 16

REFERENCES [CHAPTER 2]

1. Radiometric reporting methods and calibration in uranium exploration. Technical reports series N° 174, IAEA, Vienna 1976

2. J.A. Czubek & A. Lenda: Energy distribution of scattered gamma rays in natural gamma logging, pp. 105-116 in "Nuclear Techniques and Mineral Resources", IAEA, Vienna 1969

3. Report on the Applicability of International Radiation Protection Reccommendations in the Nordic Countries. Editor: B. Lindell. The Radiation Protection Institutes in Denmark, Finland, Iceland, Norway and Sweden. Liber Tryck, Stockholm 1976

4. Dresser Atlas. Log Review 1. Collective work, Houston 1974

5. J.A. Czubek: The Influence of the Drilling Fluid on the Gamma-Ray Intensities in the Boreholes. Acta Geophysica Polonica 10 (1962) 25-31

6. J.A. Czubek: Some Problems of the Theory and Quantitative Interpretation of the Gamma-Ray Logs. Acta Geophysica Polonica 9 (1961) 121-132

7. J.A. Czubek: Quantitative interpretation of the statical anomalies of the gamma-ray logs. Nukleonika 7, No. 5, 347-356 (1962).

8. J.A. Czubek & T. Zorski: Recent Advances in Gamma-Ray Log Interpretation. Pp. 45-86 in "Evaluation of Uranium Resources", IAEA, Vienna 1979.

9. J.A. Czubek: Differential interpretation of gamma-ray logs: I. Case of the Static Gamma-Ray Curve. Inst. Nucl. Phys. Rep. N° 760/J, Kraków, Poland 1971

10. J.A. Czubek: Differential interpretation on gamma-ray logs: II. Case of the Dynamic Gamma-Ray Curve. Inst. Nucl. Phys. Rep. N° 793/I, Kraków, Poland 1972

11. J.A. Czubek: New theory, possibilities, and practice in digital interpretation of gamma-ray logs. Paper W in "Proc. SPWLA XN-th Ann. Log. Symp., May 6-9 1973, Lafayette, Lou., U.S.A.

12. J.A. Czubek, J. Koskiewicz, J. Gyurcsak, A. Lenda, K. Umiastowski & T. Zorski: Geostatistical method of interpretation of nuclear well logs. pp. 313-332 in "Nuclear Techniques and Mineral Resources 1977", IAEA, Vienna 1977

3 NEUTRON-NEUTRON LOG

3 NEUTRON-NEUTRON LOG

J.A.C. JUNE 19, 1978

Basic physical features of the neutron log are presented in my lectures from Melbourne *[Ref. 13, 14, 15, 16]* which I have left in Orkustofnun. Here, therefore, the discussion will be limited only to the particular, Icelandic, problems.

Let us only remind that the epithermal neutron flux $\Phi_n(r)$ in the infinite homogeneous medium from a point source of fast neutrons can be given in the n-th group diffusion approximation as:

$$\Phi_n(r) = \frac{Q \cdot p}{4\pi\, \xi\Sigma_s\, L_s^3} \frac{e^{-\frac{r}{L_s}\sqrt{n}}}{2^{n-1}\,(n-1)!} \left(\frac{r}{L_s}\right)^{n-2} \cdot \tag{1}$$

$$\cdot \sum_{k=0}^{n-2} \left(\frac{r}{L_s}\right)^{-k} \frac{1}{(2\sqrt{n})^k} \frac{(n-2+k)!}{k!\,(n-2-k)!}$$

where

- Q is the neutron output from the source (n/sec)
- p is the probability for the neutron to be not absorbed during the slowing down process *[17]*
- $\xi\Sigma_s$ is the slowing down cross section for the last neutron group
- r is the source-detector distance and
- L_s is the slowing-down length defined for the point source in the infinite medium as:

$$L_s^2 = \frac{1}{\sigma}\langle r^2\rangle = \frac{1}{\sigma}\frac{\int \Phi(r) \cdot r^2 dv}{\int \Phi(r)\, dv} \tag{2}$$

where $\Phi(r)$ is the flux of neutrons with energy equal to the final energy for which the L_s value is calculated. Eq. (2) serves also for the experimental determination of the L_s value.

Eq. (1) has been derived under the simplifying assumption (which fits quite good with the experiments) that the diffusion lengths L_k in each of the k neutron groups are equal to each other.

When $n \to \infty$ eq. (1) approaches the so called Fermi age solution:

$$\Phi_{n\to\infty}(\gamma) = \frac{Q \cdot p}{(4\pi)^{3/2} L_s^3 \xi\Sigma_s} \cdot e^{-\frac{r^2}{4L_s^2}} \tag{3}$$

The parameters p, $\xi\Sigma_s$ and L_s are those which define the rock neutron properties for epithermal neutrons. All of them are very sensitive on the H_2O content (due to the anomalous neutron properties of hydrogen) and the slowing-down length L_s is always the most important among them. Let us also remark that when the source-detector distance r is expressed in the L_s units, say

$$x = \frac{r}{L_s} \tag{4}$$

one has in this case, that the neutron flux $\Phi_n(x)$ is equal to:

$$\Phi_n(x) = \text{const} \cdot \frac{p}{\xi\Sigma_s L_s^3} \cdot F_n(x) \tag{5}$$

where $F_n(x)$ is a function of x and is different for each number n of the neutron diffusion groups. The behaviour of $F_n(x)$ functions is given in fig. 1 [13] for some number of the diffusion groups.

In the well logging practice the range of x values (because of the constant r value for a given probe and a variable L_s value) is

$$1 \leq x \leq 5$$

and it happens that for the rock media n = 2 usually gives a good agreement with the experiment, and even, when the borehole is water filled, n = 1 fits pretty well with the experimental data for the x values not too small.

The question of the presence of the water filled borehole is much more complicated for the theoretical considerations [14] and we are not going to the detailed consideration of this question.

The thermal neutron flux $\Phi_{th}(r)$ distribution can be treated as an additional

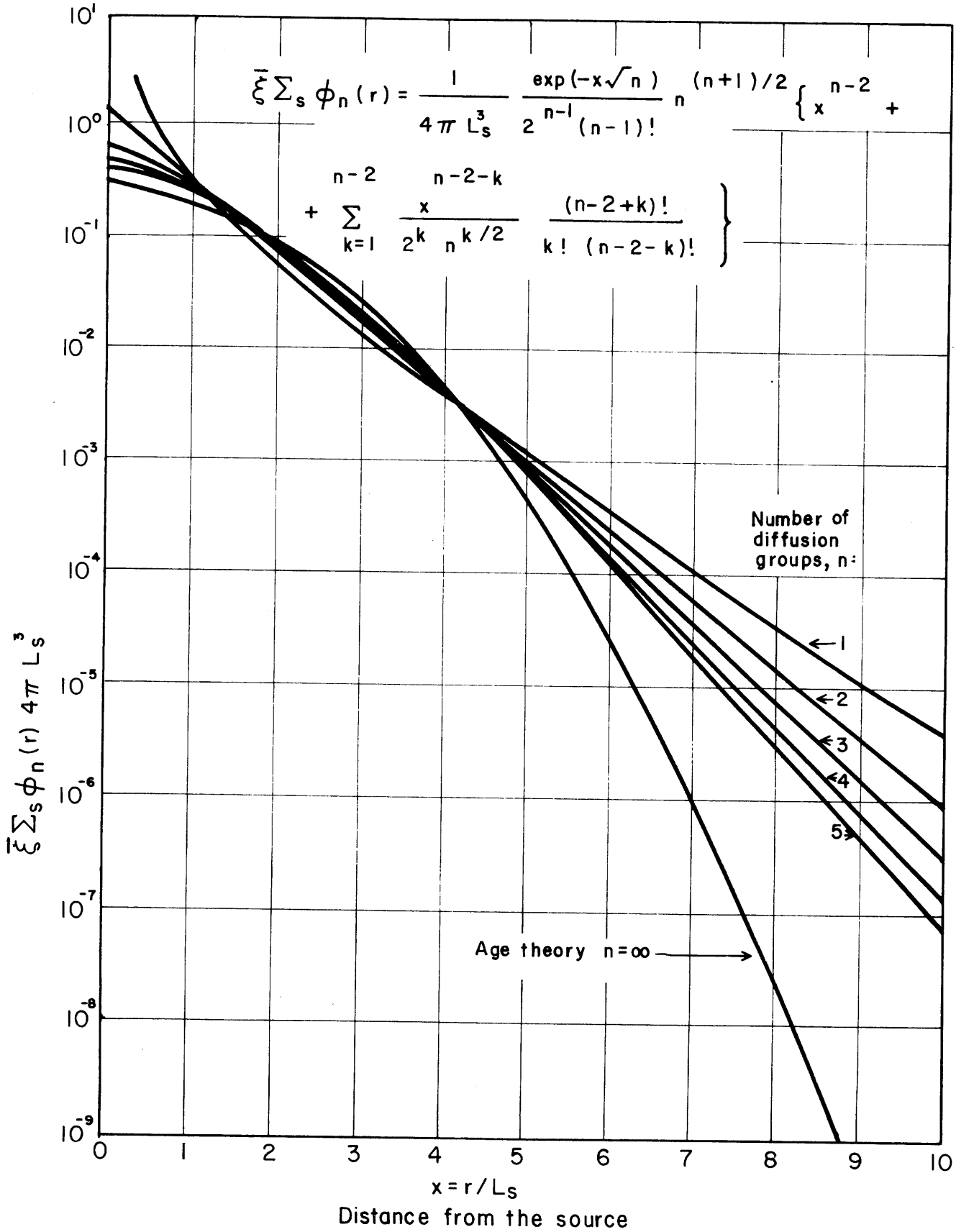

Fig. 1 *[13]*

Comparison of the neutron fluxes in multigroup diffusion approximation for the point isotropic source in an infinite medium

(thermal) diffusion group to the n groups still existing which yields to the quite complicated formula (cf. eqs. 87 and 87a in [13], which, however, gives relatively simple form when n = 1

$$\Phi_{th}(r) = \frac{Q \cdot p}{4\pi \Sigma_a r} \frac{1}{(L_s^2 - L_d^2)} \left[e^{-\frac{r}{L_s}} - e^{-\frac{r}{L_d}} \right] \tag{6}$$

and for n = 2

$$\Phi_{th}(r) = \frac{Q \cdot p}{8\pi \Sigma_a L_f^3 \alpha} \left\{ e^{-\frac{r}{L_f}} - \frac{2(1-\alpha)}{\alpha} \frac{L_f}{r} \left(e^{-\frac{r}{L_f}} - e^{-\frac{r}{L_d}} \right) \right. \tag{7}$$

here

Σ_a is the absorption cross section for thermal neutrons in the rock
L_d is the diffusion length of thermal neutrons in the rock

$$L_f^2 = L_s^2/2 \tag{8}$$

$$\alpha = 1 - L_d^2/L_s^2 \tag{9}$$

Here again, when one takes the so called migration length M for thermal neutrons:

$$M^2 = L_s^2 + L_d^2 \tag{10}$$

and the source-detector distance r is expressed in the M units, say now

$$x = \frac{r}{M} \tag{11}$$

The thermal neutron flux $\Phi_{th}(x)$ can be given as:

$$\Phi_{th}(x) = \text{const} \cdot \frac{p}{\Sigma_a L_s^3} \cdot F_{n+th}(x,\alpha) \ , \tag{12}$$

where again the space (x) behaviour of the function $F_{n+th}(x,\alpha)$ is very similar to this one of the function $F_n(x)$ given in fig. 1.

The other approach to the thermal neutron flux $\Phi_{th}(r)$ value is to treat it as a result of the space convolution of the epithermal neutron sources (i.e. the epithermal neutron flux)

$$\xi\Sigma_s \Phi_n (\bar{r}_1)$$

With the solution of the thermal neutron flux $\phi(\bar{r}_2)$ from the point thermal neutron source, like it is shown in fig. 2.

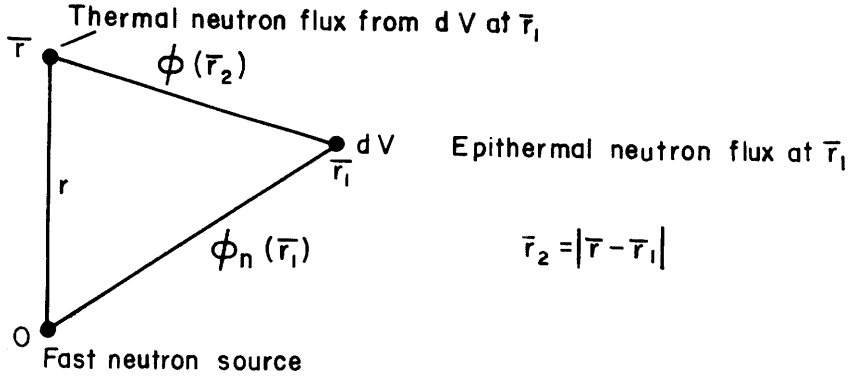

Fig. 2

that is:

$$\Phi_{th}(\ ) = \bar{\xi}\Sigma_s \int_V \Phi_n(\bar{r}_1) \cdot \phi(\bar{r} - \bar{r}_1)\, d\bar{r}_1 \qquad (13)$$

Which for the usual case when $L_s > L_d$ can be imaginated as in fig. 3

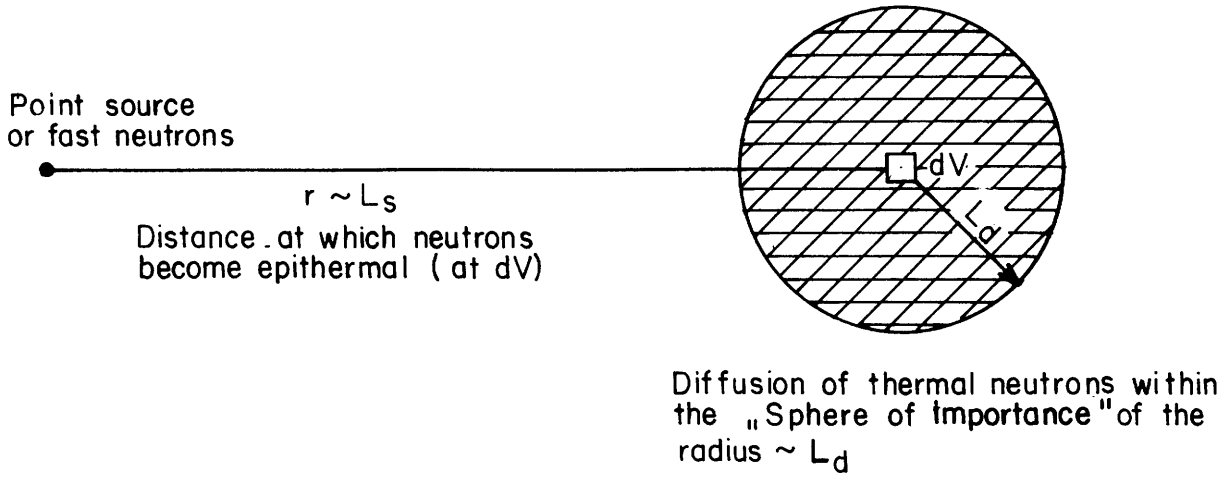

Fig. 3

Diffusion of thermal neutrons within the "sphere of importance" of the radius ~ L_d

Using this approach one can expect that the main space behaviour of the thermal neutron flux $\Phi_{th}(r)$ will be given by the space behaviour of the epithermal neutron flux $\Phi_n(r)$.

This simple physical explanation of the basic features of the neutron fluxex will permit to solve the most important problem in the neutron logging, i.e. how to know the calibration curve for a given neutron tool. In this case under the calibration curve the relationship between the neutron tool readings and the rock porosity Φ is understood.

3.1 Neutron parameters of rocks

As it can be seen from eqs. (1) ÷ (7) or from fig. 1 the neutron flux Φ_n or Φ_{th} at a given distance r from the source is defined by the neutron parameters of the rock:

for epitermal neutrons:

$$L_s,\ \xi\Sigma_s,\ p$$

for thermal neutrons:

$$L_s,\ L_d,\ p,\ \Sigma_a\ ,$$

where also the relation

$$L_d^2 = \frac{D}{\Sigma_a} \qquad (14)$$

is sometimes used, D being here the diffusion coefficient for thermal neutrons. All these parameters listed above are the functions of the rock density and its elemental composition. The quantities $L_s \cdot \rho$, $L_d \cdot \rho$, Σ_a/ρ, $\xi\Sigma_s/\rho$, $D \cdot \rho$ and p are density independent (ρ is here the bulk density of the material) and are the pure functions of the rock elemental composition. Among all neutron parameters enumerated above the slowing-down length L_s has the biggest influence on the neutron flux Φ_n or Φ_{th} when the hydrogen content of the rock is variable.

There exist many different methods of calculation of the L_s values. They are all based on different approximate solutions of the Boltzmann equation for neutron transport, and all of them try to fit the experimental data. Unfortunately, as far as rocks concerns there are very few experimental data-only for dry sandstone and limestone (measured by J. Tittman in the beginning of 1950's) and this one for pure water. The method of A. Kreft from Inst. Nucl. Phys. & Techn. in Kraków, based on the 25 diffusion group approximation and taking account of inelastic scattering *[18]* seems to be the best one.

17 averaged chemical analysis of magmatic rocks published by Daly *[19]* have been taken into account in order to find some general behaviour of igneous rocks as far as concerns their L_s values. These analyses are listed in table 1. For some technical reasons the P_2O_5 content was neglected, the total was normalized to 100% and the results were re-calculated to obtain the elemental content (not in the form of oxides) in the weight per cent. These data are presented in table 2. In this table the solid rock densities ρ_M (i.e. assuming porosity equal zero) taken for further calculations are also presented. Dr. Kreft has kindly calculated the L_s and p values on my demand, for the data in table 2. Analysing his results for the L_s values it was possible to find some approximate formula, which starting from the knowledge of the ρ_M and p_w data for the rock matrix permits to get the right L_s values for the igneous rocks. P_w is here the weight content of the chemically bounded water in the dry rock. This value was obtained as:

$$P_W = \frac{H}{0.1119} \qquad (15)$$

TABLE 1

Our nomenclature		N° of analysis and the rock nomenclature after Daly [19]		N° of samples
1.	Dunite	= 17.	Dunite	10
2.	Periodotite	= 76.	Wehrlite	5
3.	Pyroxenite	= 85.	Diallagite	14
4.	Gabbro	= 57.	All gabbro	41
5.	Basalt	= 58.	All basalt	198
6.	Diabase	= 90.	Diabase	90
7.	Diorite	= 125.	Diorite, incl. 55 quarz diorites	125
8.	Andesite	= 49.	All andesite	87
9.	Granodiorite	= 45.	All granodiorite	40
10.	Dacite	= 46.	Dacite	90
11.	Granite	= 4.	Granite of all periods	546
12.	Liparite	= 5.	Rhyolite, incl. 24 liparites	126
13.	Syenite	= 18.	All syenite, incl. 5 "alkaline"	50
14.	Trachyt	= 19.	Tirachyts, as named by authors	48
15.	Nephel. syenite	= 40.	Nephelite syenite	43
16.	Phonolite	= 41.	Phonolite	25
17.	Urtite	= 35.	Urtite	3

where H is the weight per cent of hydrogen reported in table 2. This, called by us "correlation" formula, is:

$$L_s = \frac{1}{\rho} \times [m \lg_{10} H_2O + b] \tag{16}$$

$$\rho = (1 - \Phi)\ \rho_M + \Phi = (1 - \frac{H_2O}{100}) \cdot \rho_o + \frac{H_2O}{100} \tag{17}$$

$$\begin{aligned} m &= -\alpha_1 \cdot b - \beta_1 \\ \alpha_1 &= 0.37324213 \\ \beta_1 &= 5.041956467 \end{aligned} \tag{18}$$

TABLE 2

ELEMENTAL COMPOSITION (WEIGHT PER CENT) OF IGNEOUS ROCKS (AFTER DALY)

(2200 m/s)	σ_ξ(barns)	0.16	5.8	0.243	2.62	0.069	0.44	0.525	2.07	0.332	~0
	ρ_M g/cm^3	Si %	Ti %	Al %	Fe %	Mg %	Ca %	Na %	K %	H %	O %
		0	1	2	3	4	5	6	7	8	9
1. Dunite	3.28	18.96	0.01	0.46	6.31	28.00	0.50	0.07	0.03	0.32	45.34
2. Peridotite	3.23	21.14	0.38	3.06	9.85	13.86	5.37	0.85	0.47	0.35	44.67
3. Pyroxenite	3.23	22.00	0.58	3.38	11.32	7.34	11.49	0.61	0.41	0.11	42.76
4. Gabbro	3.0	22.63	0.58	9.50	6.86	4.55	7.89	1.90	0.74	0.16	45.19
5. Basalt	3.0	23.10	0.82	8.37	8.78	3.75	6.44	2.33	1.27	0.18	44.96
6. Diabase	3.0	23.70	0.87	8.15	8.77	3.51	6.42	2.29	0.81	0.21	45.27
7. Diorite	2.84	27.63	0.46	8.75	5.18	2.16	4.40	2.58	1.76	0.14	46.94
8. Andesite	2.60	27.96	0.46	9.20	4.78	1.67	4.16	2.67	1.70	0.14	47.26
9. Granodiorite	2.72	30.45	0.34	8.46	3.29	1.15	3.17	2.75	2.29	0.12	47.98
10. Dacite	2.6	30.75	0.34	8.62	3.15	0.85	2.48	2.95	2.22	0.17	48.47
11. Granite	2.67	32.89	0.24	7.68	2.49	0.53	1.43	2.59	3.42	0.09	48.64
12. Liparite	2.6	34.07	0.20	7.15	1.70	0.23	0.86	2.51	3.71	0.16	49.41
13. Syenite	2.75	28.24	0.40	8.65	4.49	1.51	3.09	2.96	3.74	0.13	46.79
14. Trachyt	2.60	28.43	0.23	9.41	3.89	0.68	2.22	3.30	4.78	0.14	46.92
15. Nephesyenite	2.75	25.68	0.52	10.59	4.09	0.53	1.80	6.16	4.56	0.15	45.92
16. Phonolite	2.6	26.91	0.25	10.93	2.45	0.18	1.07	6.57	4.35	0.23	47.06
17. Urtite	2.6	21.34	0.00	14.71	2.96	0.12	1.24	12.07	3.09	0.05	44.42
$\xi\sigma_s$ (b/Δv)		0.199	0.224	0.131	0.523	0.369	0.192	0.340	0.131	14.2	0.584
$\frac{\xi\sigma_s}{A_i}$ (b/Δv)		$7.085\cdot10^{-3}$	$4.676\cdot10^{-3}$	$4.855\cdot10^{-3}$	$3.365\cdot10^{-3}$	$1.518\cdot10^{-2}$	$4.790\cdot10^{-3}$	$1.479\cdot10^{-2}$	$3.350\cdot10^{-3}$	14.088	$3.650\cdot10^{-2}$

$$b = \rho_{0.01} \times [m_1 \cdot \rho_{0.01} + b_1]$$
$$m_1 = -5.974367982 \qquad (19)$$
$$b_1 = 41.99660678$$

$$\rho_{0.01} = 0.99 \times \rho_o + 0.01 \qquad (20)$$

$$\rho_o = \frac{\rho_M - \frac{\rho_M \cdot P_w}{100}}{1 - \frac{\rho_M \cdot P_w}{100}} \qquad (21)$$

$$H_2O = (\Phi + \frac{P_w \cdot \rho_M}{100}) \times 100 \quad [\%] \qquad (22)$$

here the notation is:

- Φ - Water saturated rock porosity in the ratio of 1.0 (i.e. $0 \leq \Phi \leq 1.0$)
- ρ - Rock bulk density (g/cm^3)
- ρ_o - Apparent rock density when the chemically bounded hydrogen is "taken out" assuming it is in the form of water
- $P_w \cdot \rho_M$ - Volume content (in per cent when P_w is also in per cent) of the chemically bounded water
- H_2O - Total water content (i.e. chemically bounded plus porous water) per volume (in per cent)
- α_1, β_1, m_1 and b_1 - Coefficients found from the correlation between the exact method of calculation after Kreft and the formula (16).

The comparisons between the exact (after Kreft) values of L_s and those obtained using eqs. 16 ÷ 22 are given in figs. 4, 5 and 6 for three different porosities: Φ = 0%, Φ = 20% and Φ = 40%. To simplify the presentation of data the L_s values for igneous rocks have been calculated after eq. 16 taking ρ_o as the parameter and one can see that usually the accuracy of eq. 16 is better than 0.1 cm.

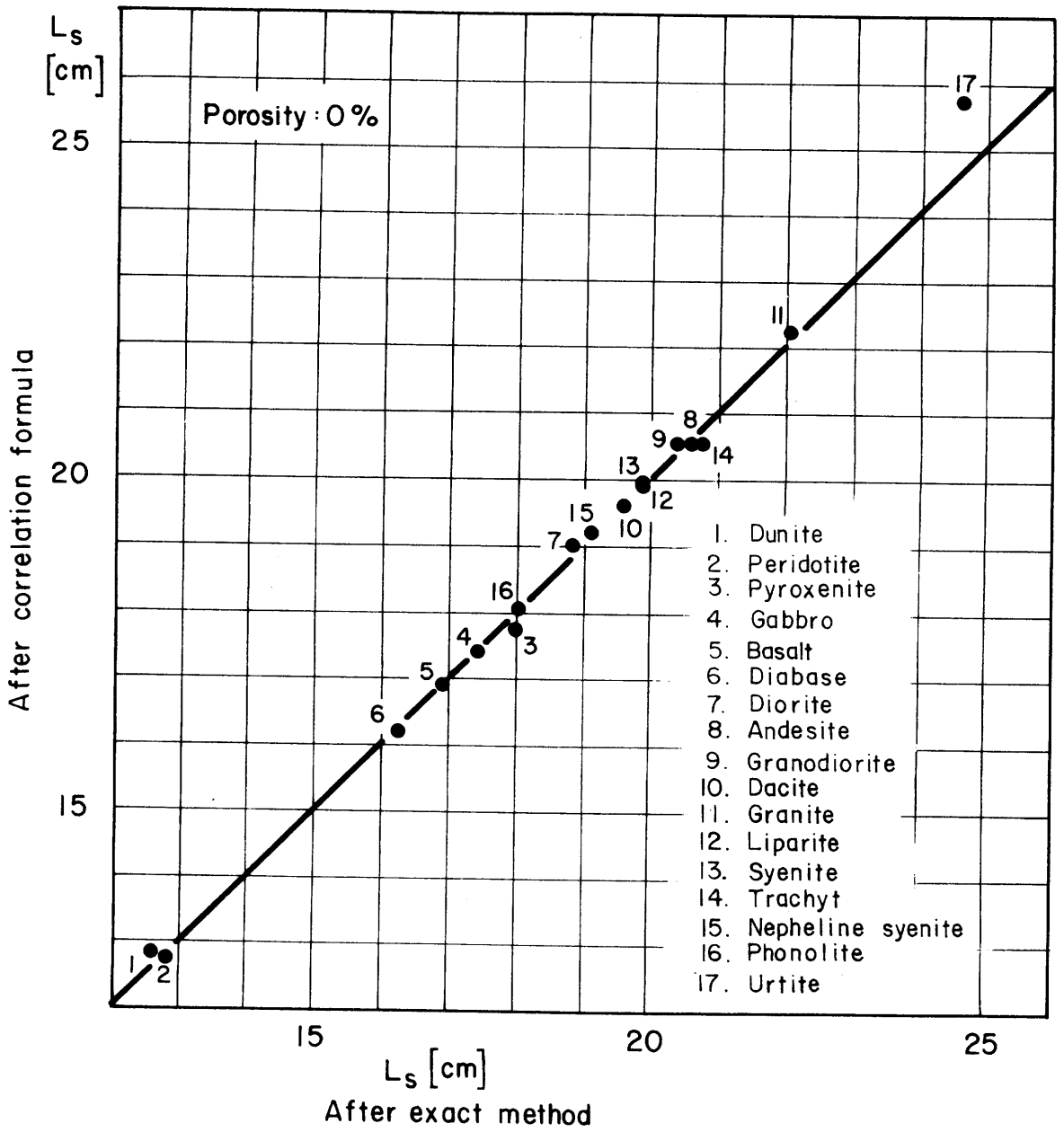

Fig. 4

After exact method

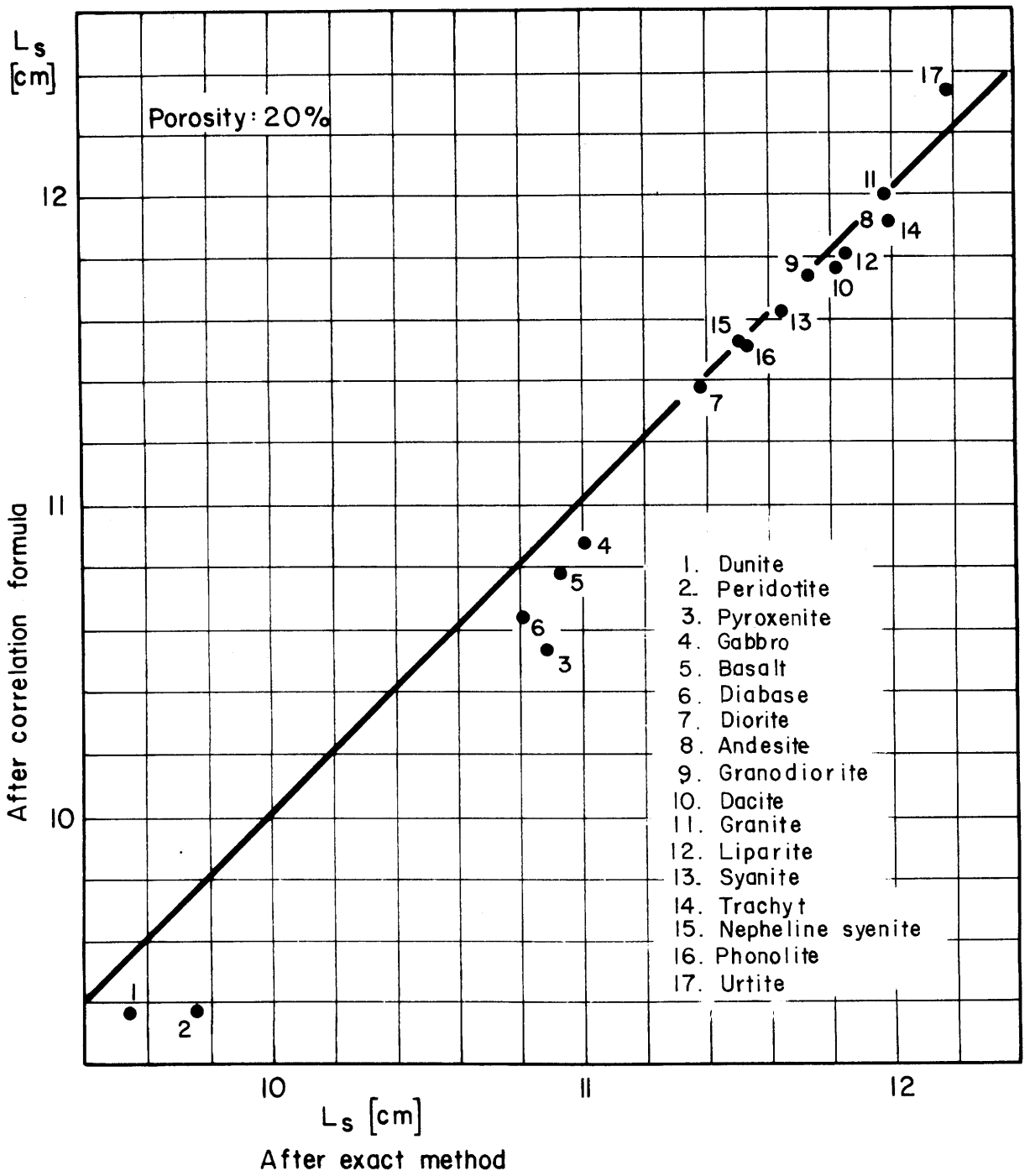

Fig. 5

After exact method

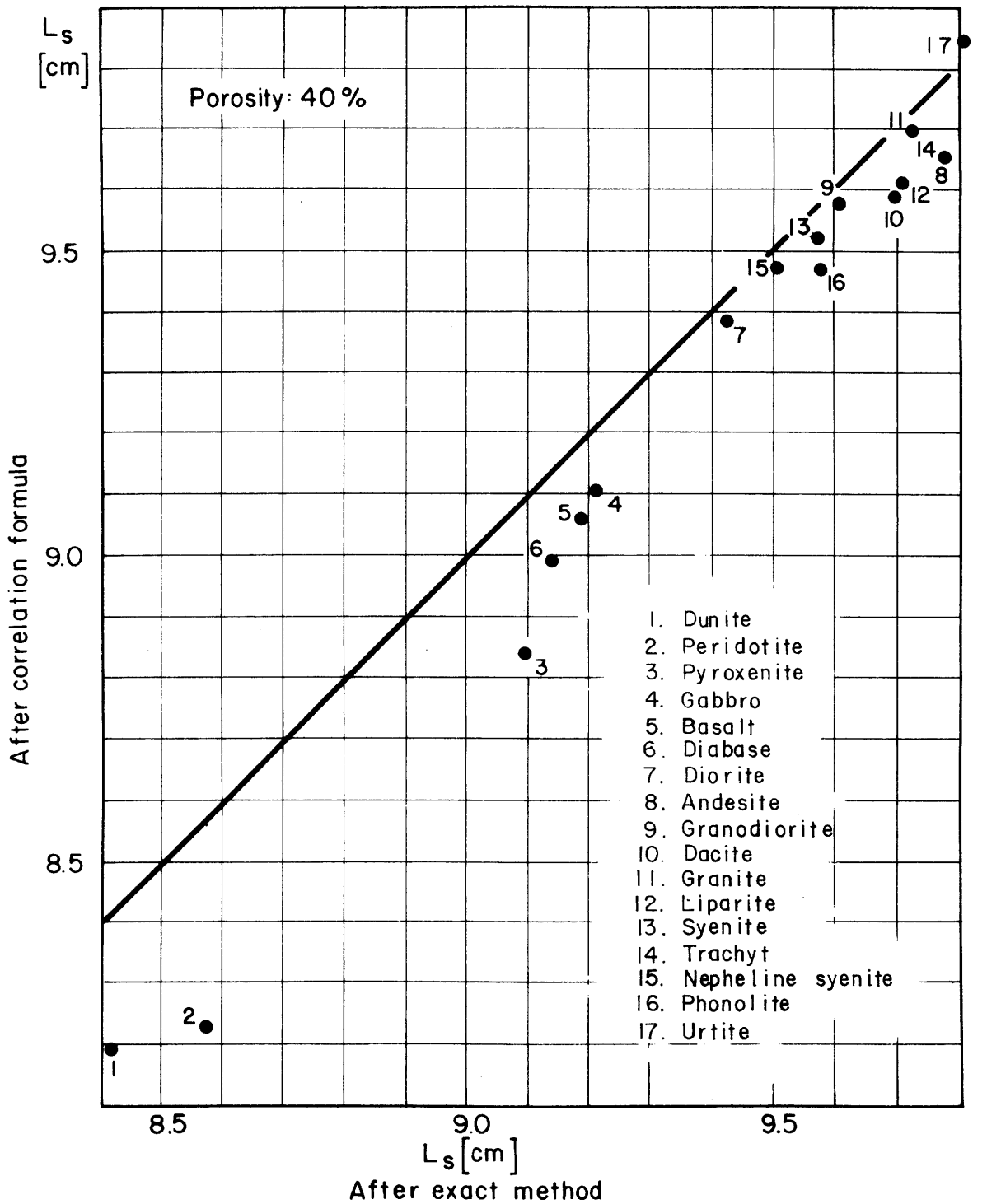

Fig. 6

After exact method

calling the value $H_2O = \Phi + P_w \cdot \rho_M$ as the rock porosity (which should be rather called the porosity index). The results are presented in figs. 7 and 8 for the ρ_o range from $\rho_o = 2.60$ g/cm^3 to $\rho_o = 3.60$ g/cm^3. In fig. 7 the L_s values are in $\log_{10}$ scale to obtain better graphic resolution of the plot. In fig. 8 the L_s values for limestone (after Kreft ref. 18) are also plotted.

When one compares the L_s values of igneous rocks for $\rho_o = 2.65$ g/cm^3 with those given by Kreft *[18]* for the sandstone of the same mineralogical density ρ_o one finds that at least within the range from 2 to 45% of porosity the igneous rocks and the sandstone have the same L_s values.

Looking next on eq. 5 one has tried to fit the density independent parameter

$$\frac{p}{\overline{\xi\Sigma}_s \cdot L_s^3 \cdot \rho_M^2}$$

for the igneous rock (in function of the weight water content P_w) to the same parameter but for pure SiO_2 and H_2O. The corresponding $\overline{\xi\Sigma}_s$ values for particular elements needed for this calculation are given in the last row of table 2. The results are given in fig. 9. Here again all igneous rocks fit quite well one straight line defined as

$$\frac{p}{\overline{\xi\Sigma}_s \quad L_s^3 \quad \rho_M^2} = m \cdot P_w + b$$

$$m = 5.312918 \times 10^{-5} \text{ cm}^4 \text{ g}^{-2} (\%W)^{-1} \qquad (23)$$

$$b = 1.44251 \times 10^{-4} \text{ cm}^4 \text{ g}^{-2}$$

with the correlation coefficient

$$r = 0.979696$$

and the pure quartz can be considered as belonging to this correlation. Thus, as far as concerns the epithermal neutron flux the conclusion is that the igneous rocks can be considered as having the elemental composition equivalent to this one of sandstone with, however, different

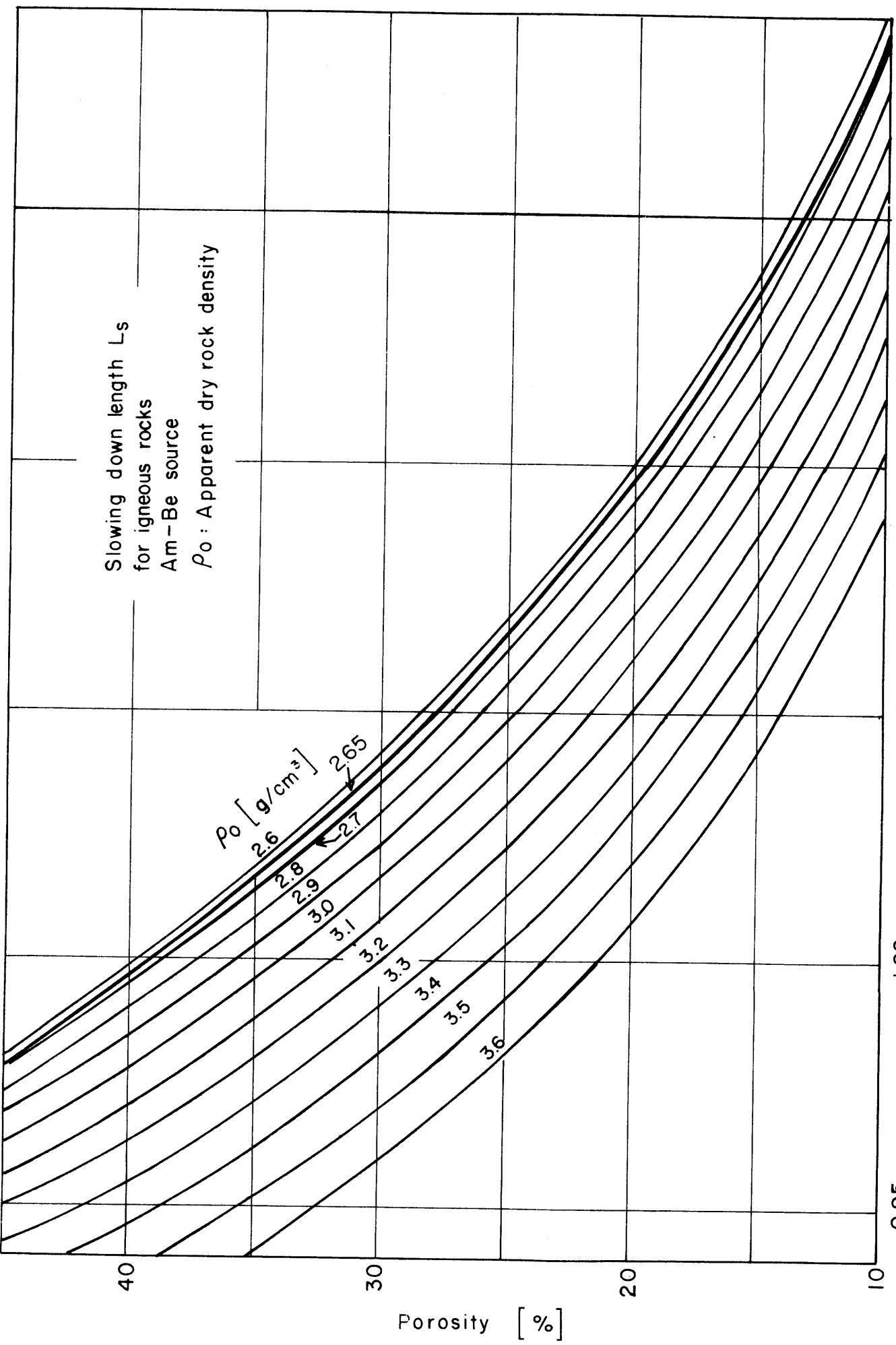

Fig. 7

Slowing down lengths L_s for igneous rocks, Am-Be source

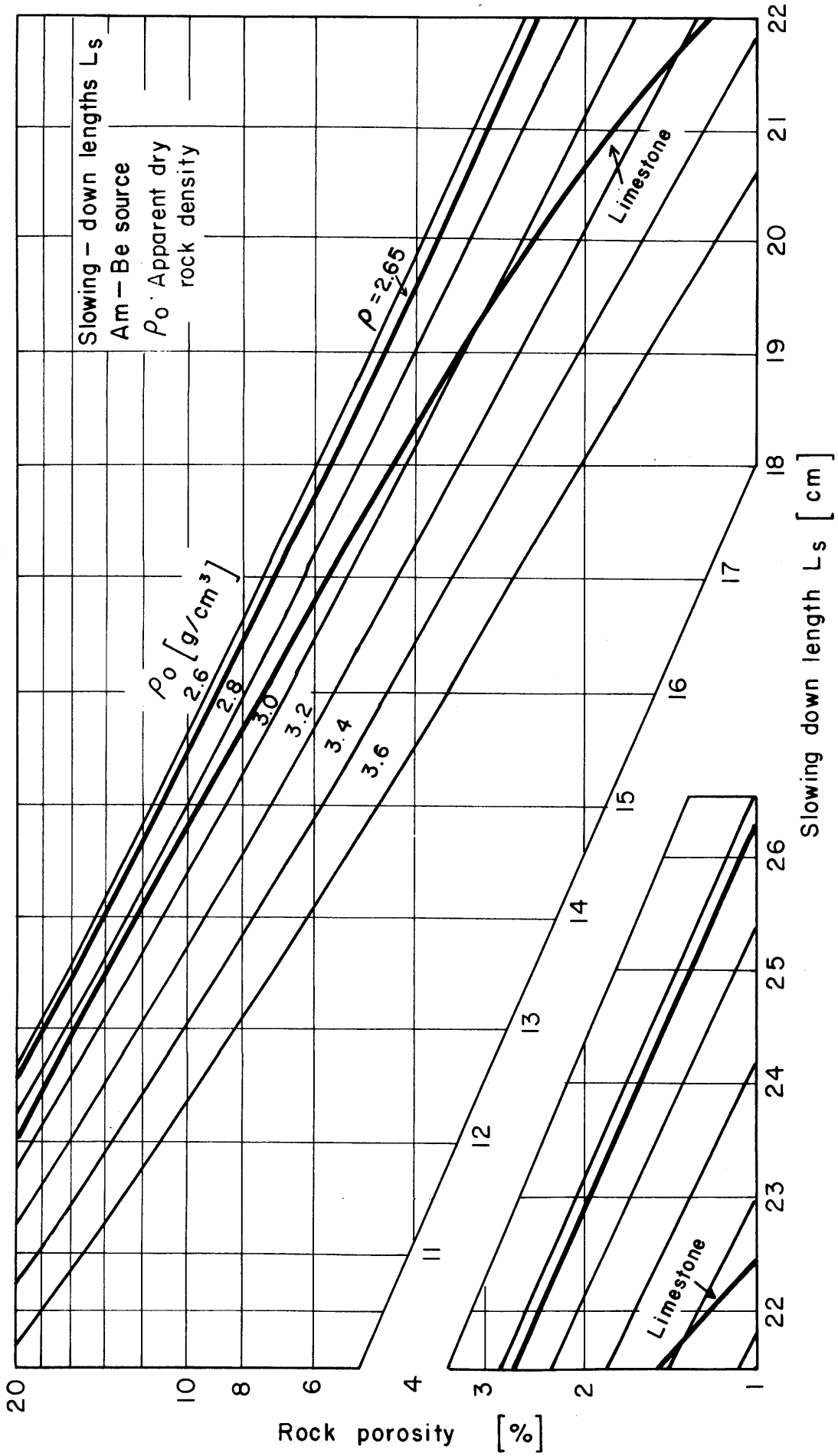

Fig. 8

Slowing-down lenghts L_s. Am-Be source

apparent mineralogical densities ρ_o. The chemically bound water in igneous rocks should be in this approach considered as a part of the porosity water of this apparent sandstone of mineralogical density ρ_o.

The thermal neutron paramters L_d, Σ_a and D have been calculated for the magmatic rocks in table 2 by Dr. J. Wozniak from the Inst. Nucl. Phys. & Techn. of Mining Academy in Kraków after the method given in ref. 20. Here it was possible to fit the Σ_a/ρ values to the linear relation:

$$\Sigma_a/\rho = m_2 \cdot H_2O + b_2 \qquad (24)$$

where ρ and H_2O are defined in eqs. 17 and 22, but the problem was that the value m_2 being relatively constant ($7.6 \times 10^{-5} \frac{cm^2}{g \cdot \%} \leq m_2 \leq 8.9 \times 10^{-5} \frac{cm^2}{g \cdot \%}$) gave more or less the same increase of $\Sigma a/\rho$ value per 1 per cent of H_2O, whereas the b_2 value was very unstable (1.96×10^{-3} $cm^2/g \leq b_2 \leq 4.00 \times 10^{-3}$ cm^2/g). Such behaviour is quite obvious for the thermal neutron absorption cross section because m_2 being mainly connected to the water absorption cross section, the b_2 value depends upon the absorption cross section of the dry rock matrix (chemically bounded water excluded). With the σ_a values (microscopic absorption cross section for thermal neutrons) so variable for different constituents of the magnatic rocks (cf. the very upper row of table 2) it gives just the b_2 values so unstable.

It was also possible to fit the $D \cdot \rho$ values to the relation:

$$\rho \cdot D = m_3 \cdot \log_{10} H_2O + b_3 \qquad (25)$$

with the relatively constant m_3 and b_3 values for all magnatic rock from table 2 ($m_3 \approx -2.0$, $b_3 \approx 4.0$ g/cm^2), thus in general, for a particular magmatic rock it is possible to calculate its L_d value from the formula

$$L_d = \sqrt{\frac{m_3 \cdot \log_{10} H_2O + b_3}{m_2 \cdot H_2O + b_2}}, \qquad (26)$$

but because of the very variable b_2 value eq. 26 cannot be used as the general formula with the parameters m_2, m_3, b_2 and b_3 constant for all types of magmatic rocks.

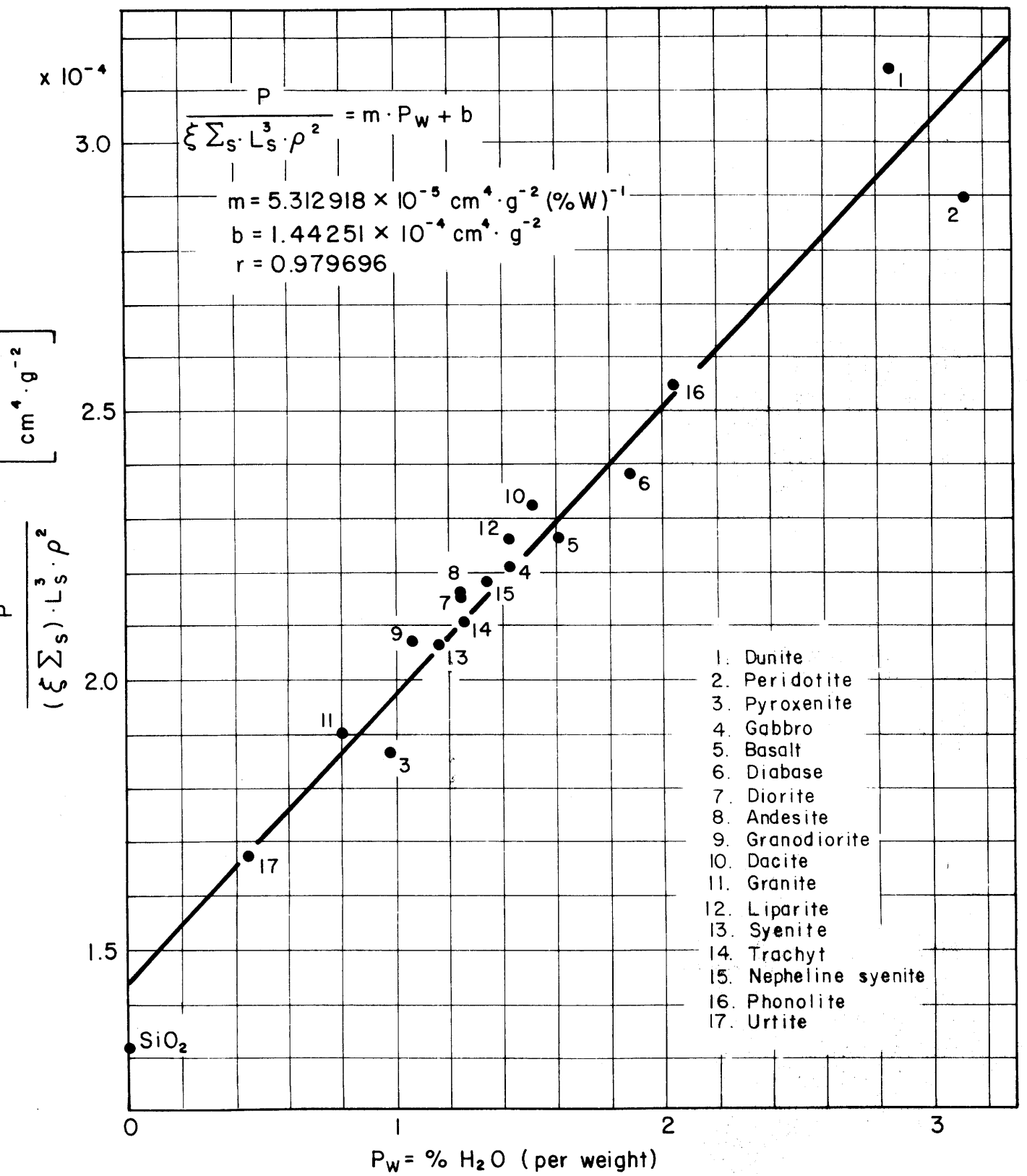

Fig. 9

P_w = % H_2O (per weight)

For the reasons presented above we shall use in our further considerations the L_s values only and the approach explained in fig. 3 to find the proper calibration curve for the neutron probe in magmatic rocks.

3.2 Neutron calibration curves

In any neutron log the probe readings are always in counts per second. This intensity is converted into the so called API neutron units. 1000 API neutron units is defined as the response of the particular neutron logging tool in the 19% porosity Indiana Limestone inside the water filled 7 7/8" borehole situated at the University at Houston. Special field calibrators delivered together with each neutron tool permit to convert the tool response in cps into the API units according to the procedure described in the Operators Manual.

For each particular probe the calibration curve i.e. tool response in API units vs. porosity is always given for the limestone lithology and for the particular borehole conditions. For the GOI 1 11/16" neutron probe these calibration curves are given in figs. 11, 12 and 13 [21]. They are given for the borehole diameter 7 7/8" only. The influence of the variable borehole diameter on the neutron probe response can be calculated using very sophisticated mathematical approach [14].. However, the general behaviour is, that if the borehole diameter is increased, the neutron probe response is decreased in a logarithmic way, i.e.

$$\lg I_{nn} = m_4 \cdot 2R + b_4 \tag{27}$$

where 2R is the borehole diameter, I_{nn} is the normalized (in API units) neutron probe response and m_4 and b_4 are particular constants for a given probe construction. Eq. 27 holds to some range of the borehole diameter 2R around the nominal value, which in our case should be taken as 2R = 7 7/8". Thus, the problem is to know the value:

$$m_4 = \frac{d}{d(2R)} \lg I_{nn} \qquad \left[\frac{\Delta \lg I_{nn}}{1"}\right] \tag{28}$$

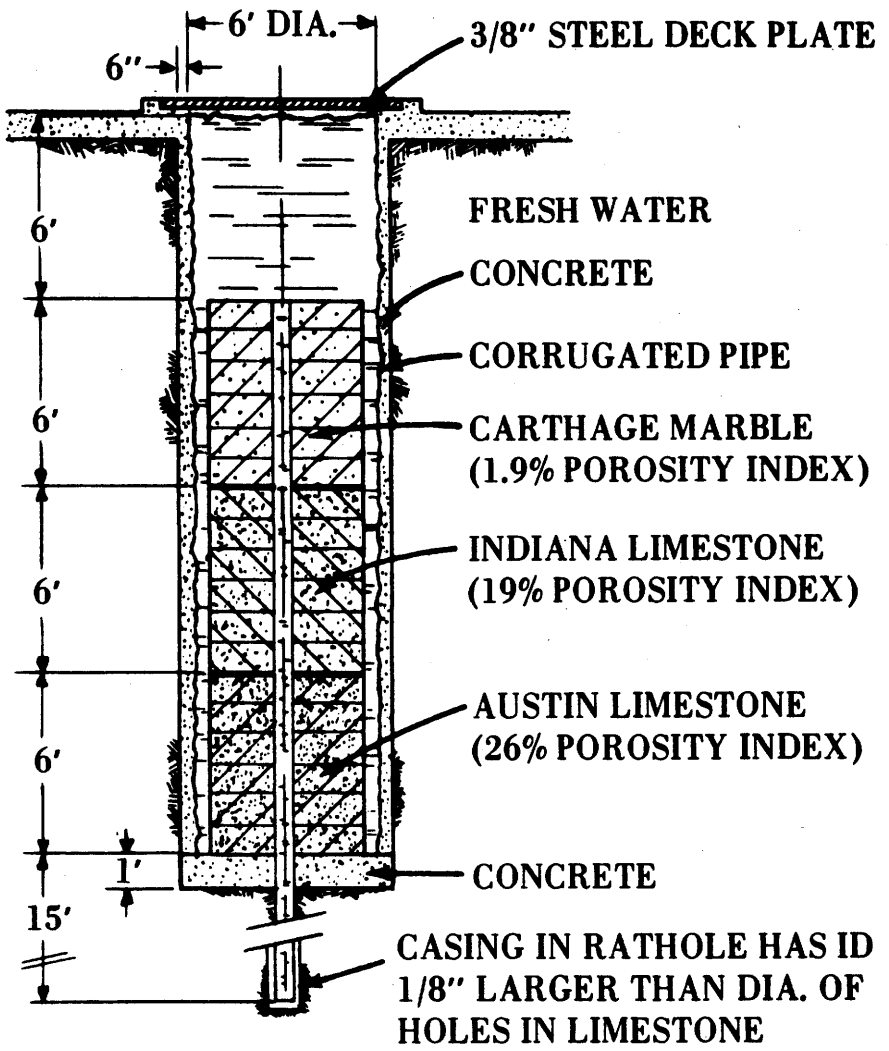

Carthage marble, Austin limestone, and Indiana limestone sections are each composed of 6 regular octagonal blocks, 5 ft. across, 1 ft. thick, with 7-7/8" (±1/16") center bore hole.

Fig. 10

A.P.I. calibration pit for neutron tools

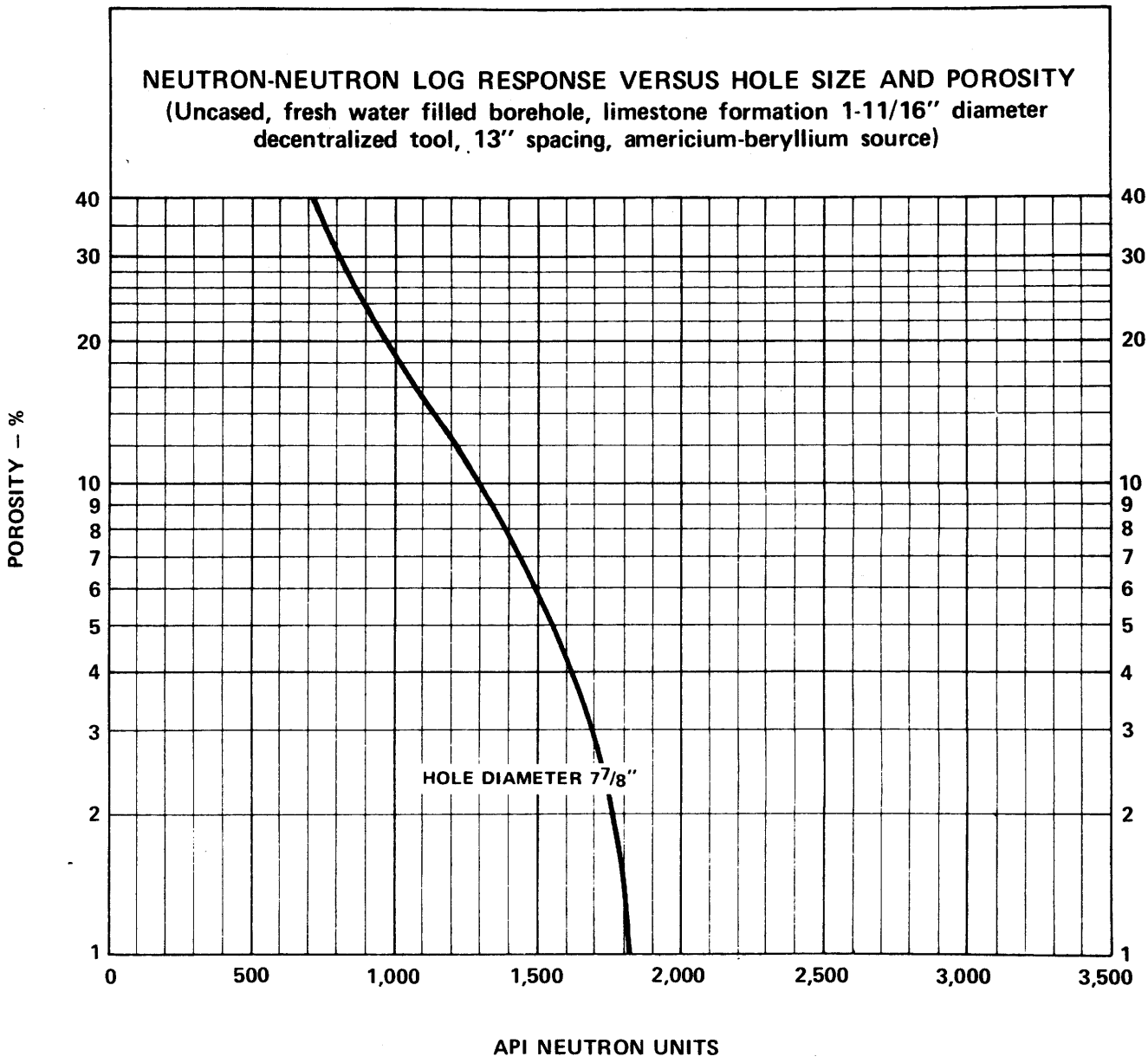

Fig. 11

API neutron units

Let m_4 be known as

$$m_4 = \frac{\Delta \lg I_{nn}}{1"} = \frac{\lg I_{nn}(R_2) - \lg I_{nn}(R_1)}{\underbrace{2R_2 - 2R_1}_{1"}} \qquad (29)$$

i.e. as the decrease of the logarithm of the neutron probe response when the borehole diameter is increased by one inch. In this case when as $2R_1$ one takes the nominal diameter (7 7/8" = 7.875") for which the probe response $I_{nn}(R_1)$ is known, one has from eq. 29:

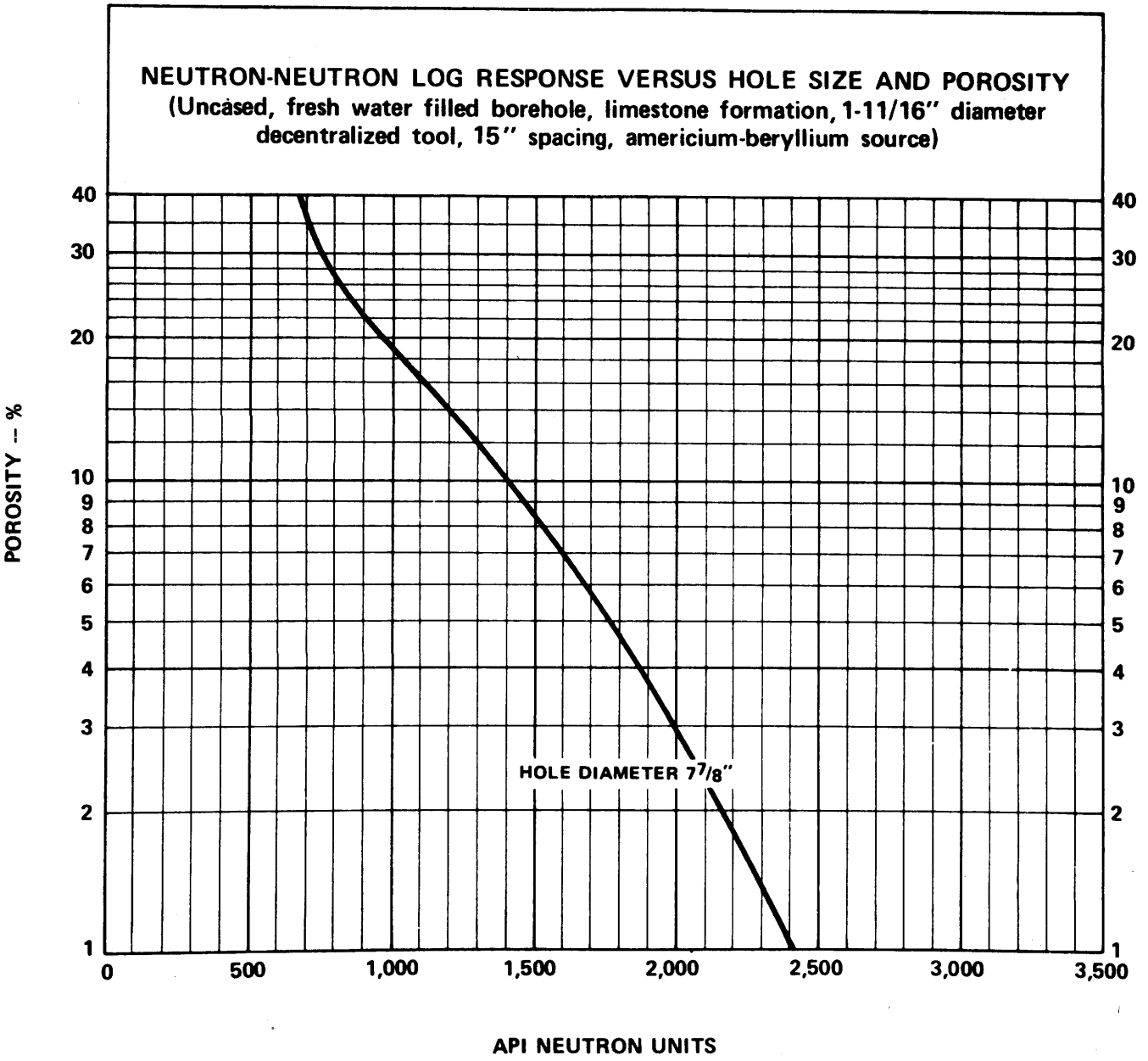

Fig. 12

API neutron units

$$I_{nn}(R_2) = I_{nn}(R_1) \times 10^{m_4 (2R_2 - 2R_1)} \qquad (30)$$

Where $2R_2$ is the new borehole diameter for which the probe response $I_{nn}(R_2)$ is sought.

The coefficient m_4 is a function of the rock porosity and of source-detector spacing and the probe construction (kind of detector, kind of shielding, etc.), thus it should be known just for a given, particular

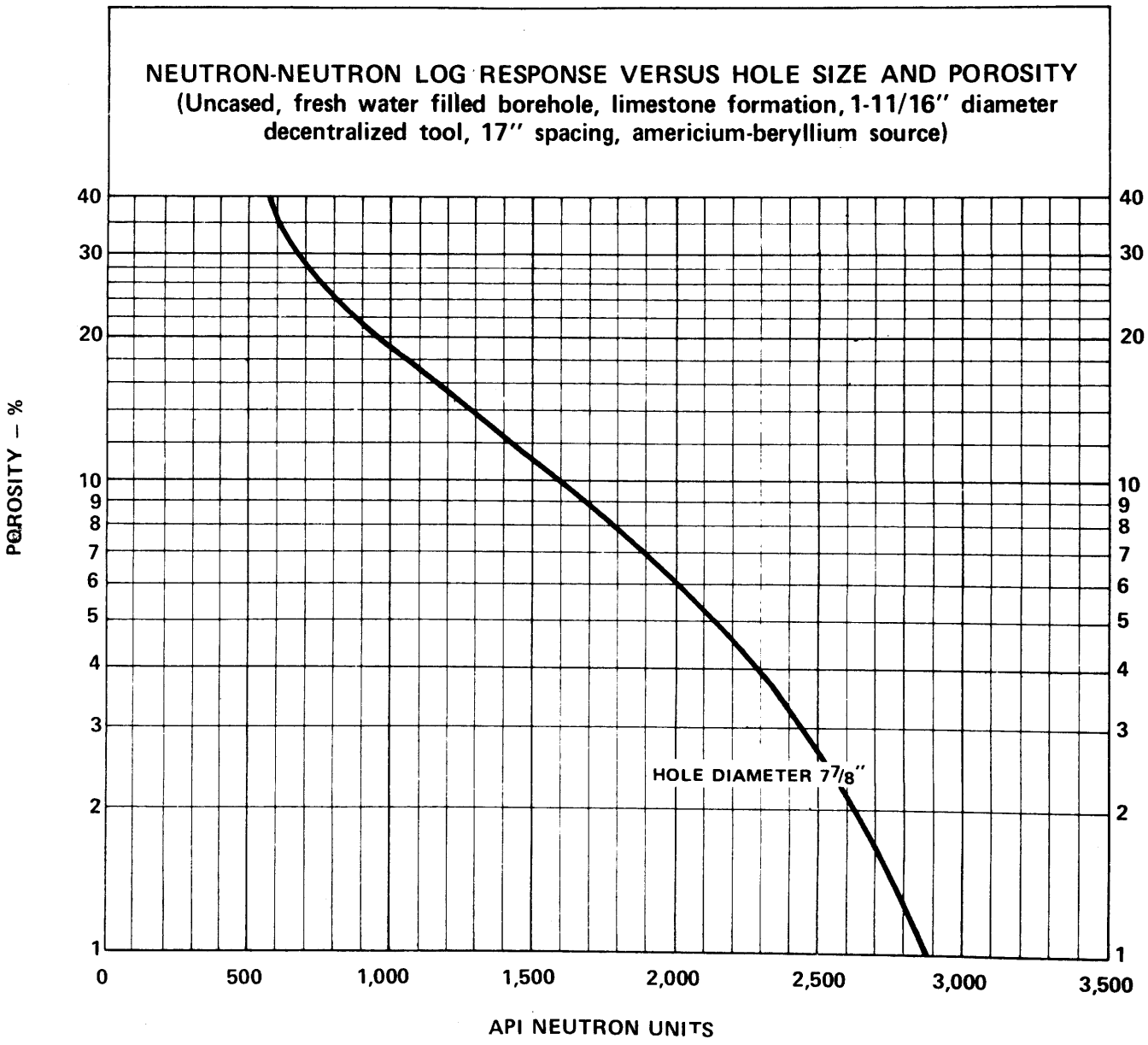

Fig. 13

API neutron units

probe, which was not our case, of course. The only available information was on the GOI neutron probe of 3 1/2" diameter and 15" spacing and on the Schlumberger GNT 1 11/16" probe, 16" spacing [21, 22]. The corresponding calibration curves are reproduced in figs. 14 and 15.

The m_4 values have been calculated from figs. 14 and 15 after eq. 28. They are reported in fig. 16. The big difference between these two kinds of neutron probes is easily visible. The 3 1/2" GOI probe is much more sensitive to the borehole diameter variations than the Schlumberger one.

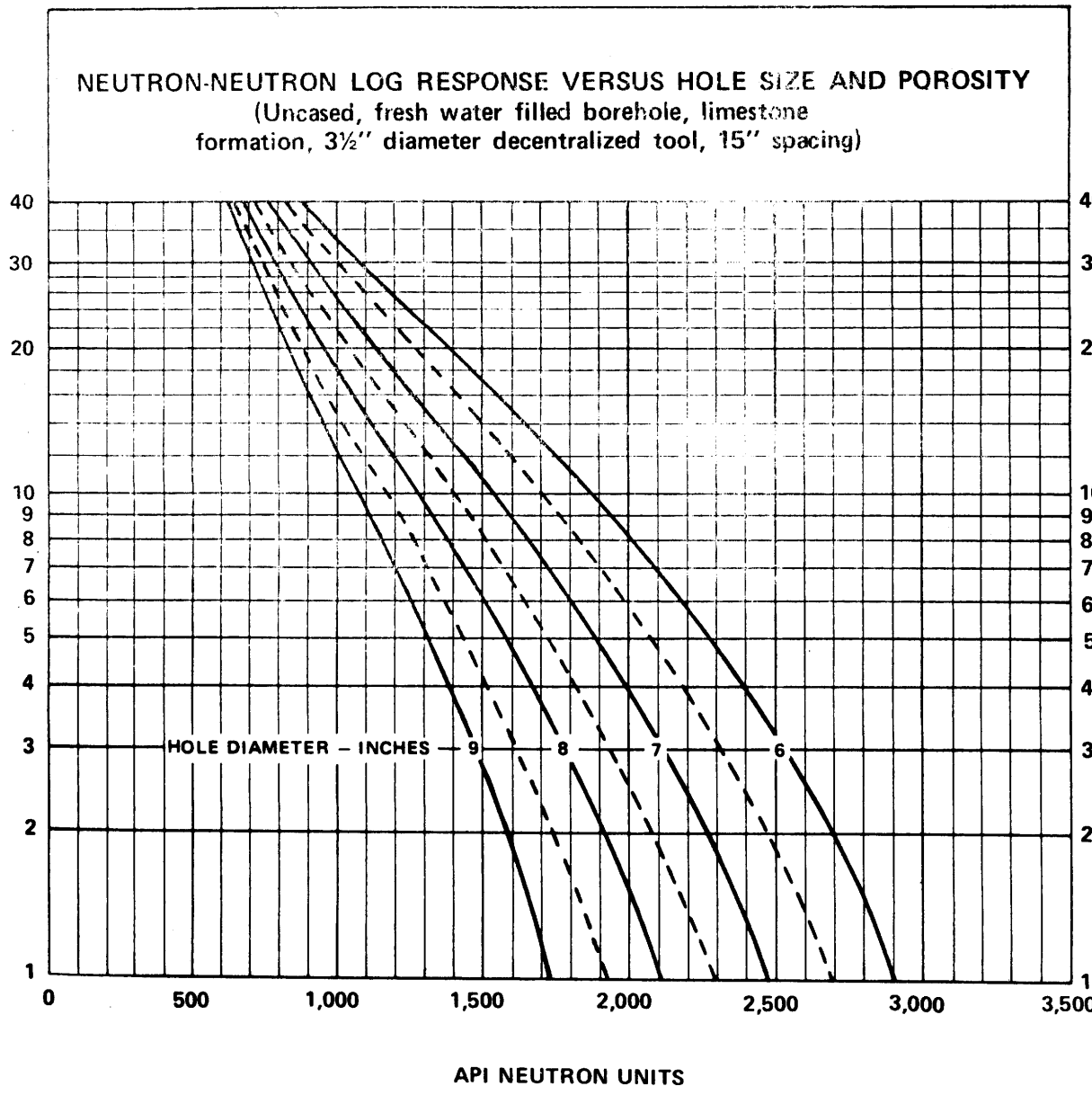

Fig. 14

API neutron units

It can be due to the differences in the probe diameter (which should, however, be to the opposite direction, in the source-detector spacing and the most probable is that it is mainly due to the difference in the internal probe construction. Having, however, this kind of information available only, one can try to establish the calibration curves for the GOI 1 11/16" NN probe using the m_4 values from fig. 16. In this way one obtains two families of calibration curves. As an example this has been carried out for the 15" spacing probe (fig. 12) using eq. 30 and the plots of the m_4 values in fig. 16, the results are presented in figures 17 and 18. When one uses these charts for interpretation, the resulting porosities will be quite different. For example for 6" borehole and 2000 API units one obtains either 9.5%

Pu-Be or Am-Be Source, 16" Spacing

FRESH MUD, UNCASED HOLES, LIMESTONE

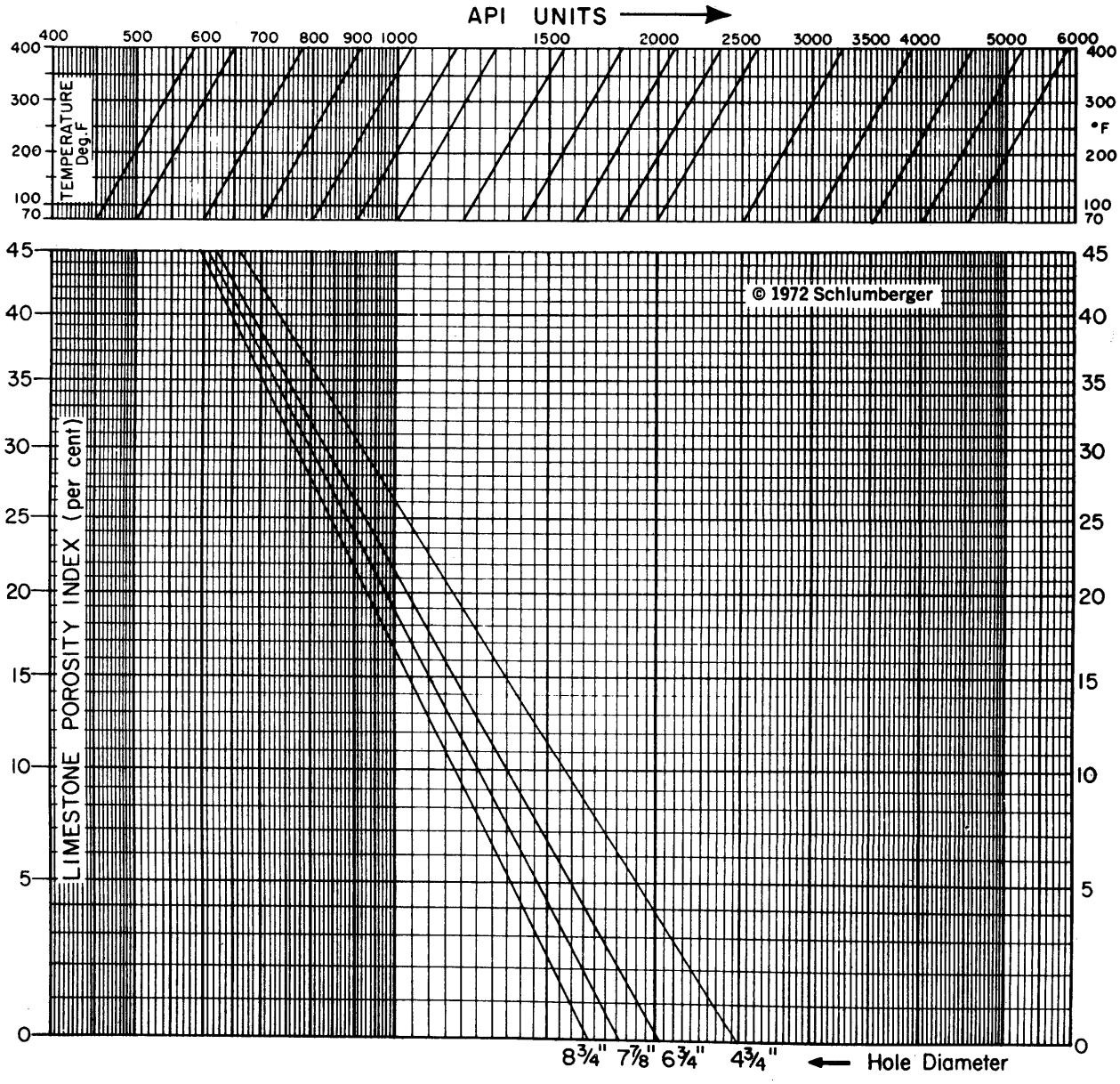

Fig. 15

Neutron departure curves GNT J, K - 1 11/16" sonde

of porosity (fig. 17) or 5.5% of porosity (fig. 18). These differences in interpretation are much more pronounced in higher porosities. The accumulation of enough field results will permit to answer which interpretation chart reflects better the real porosity of the investigated layers. Similar calibration curves should be calculated for the spacings 13" and 17".

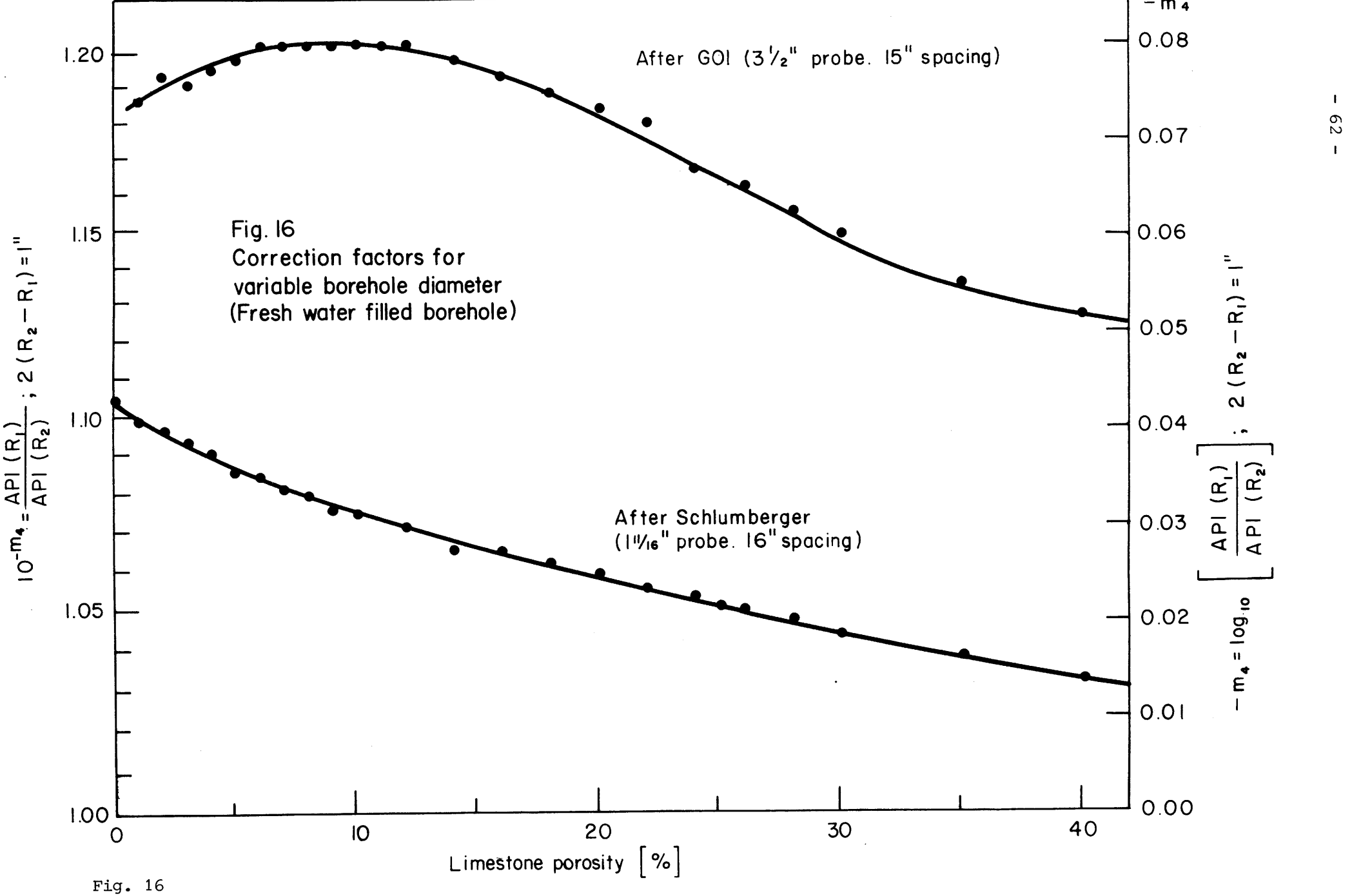

Fig. 16

Limestone porosity *[%]*

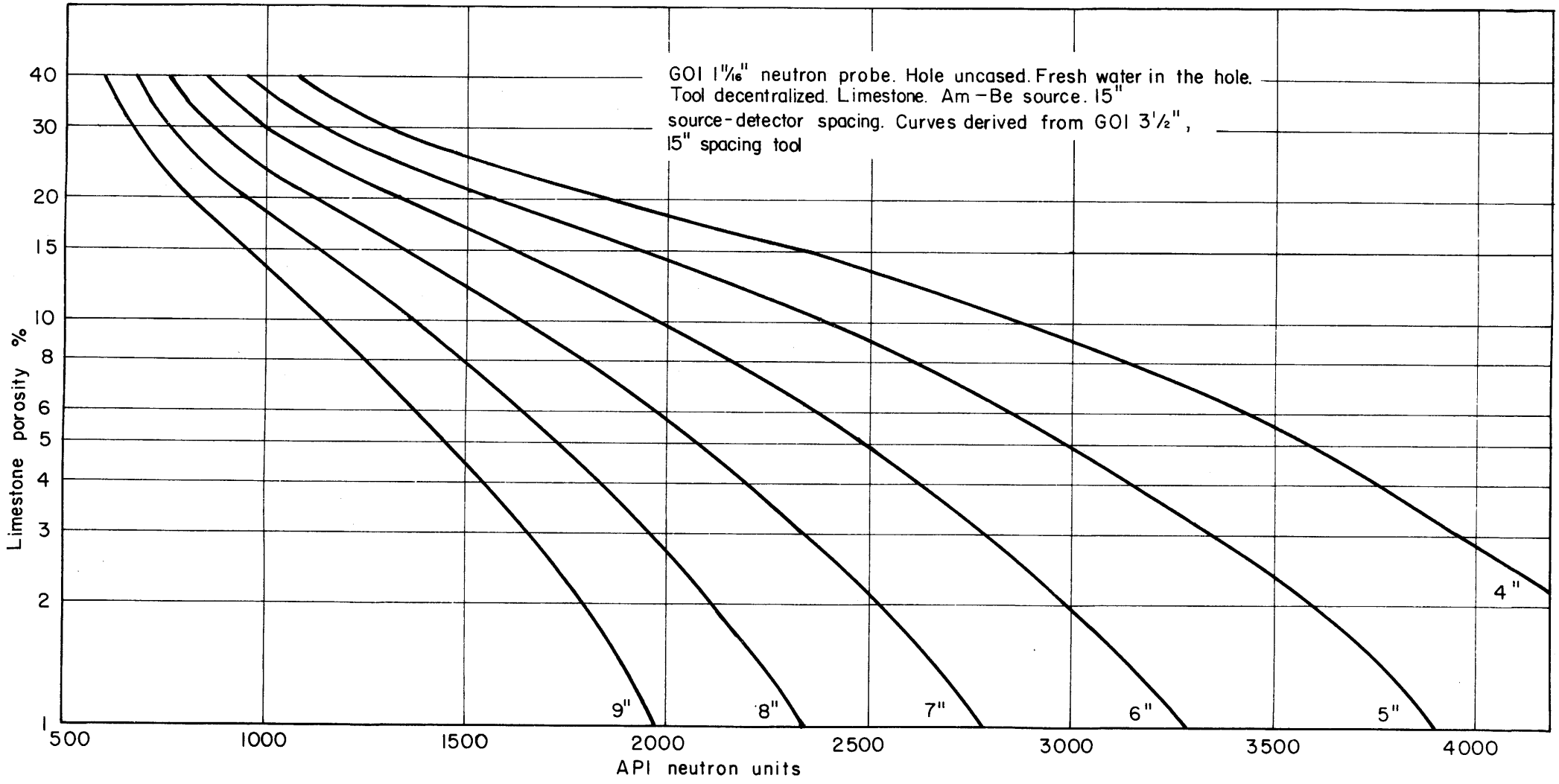

Fig. 17

API neutron units

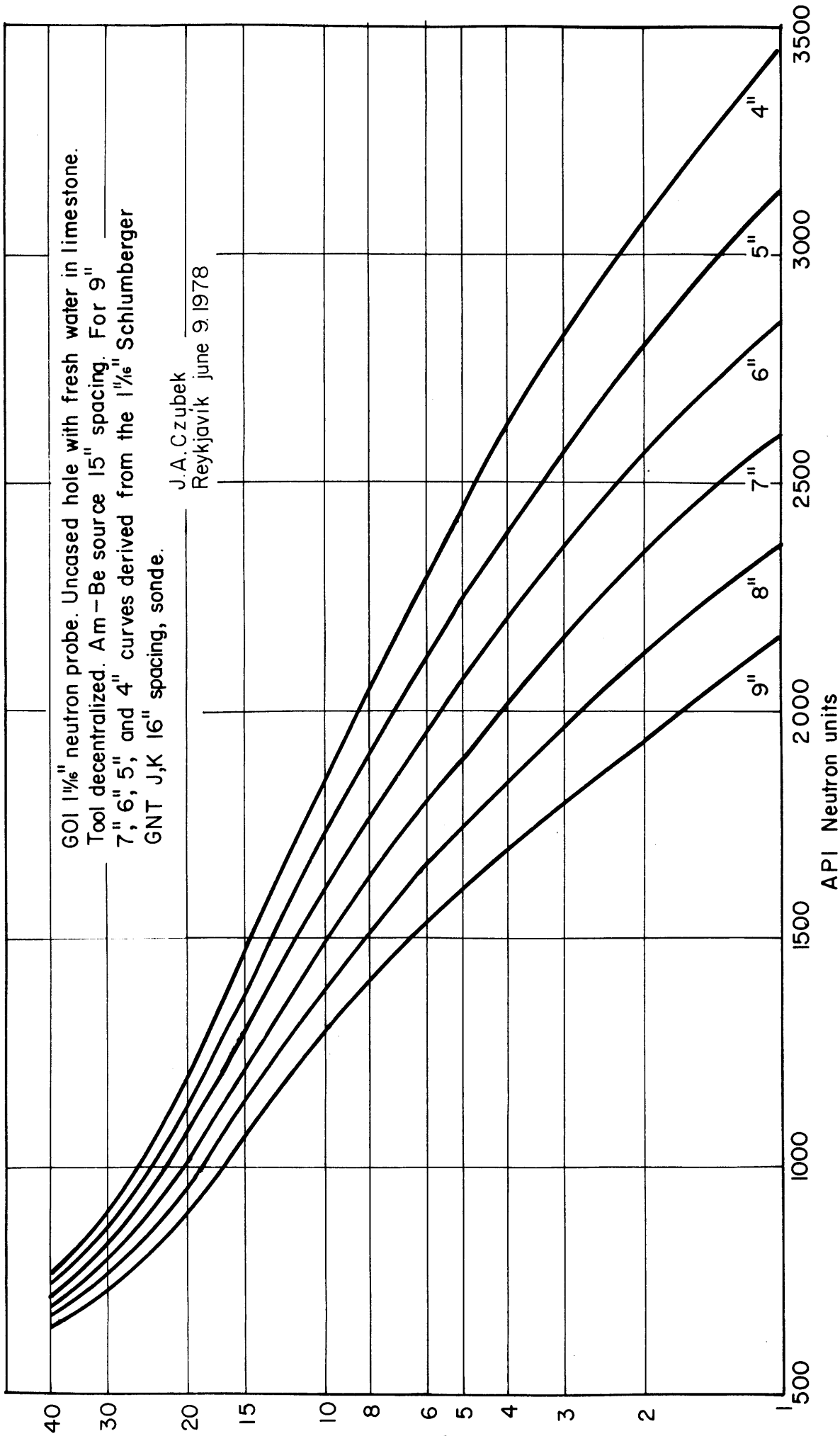

Fig. 18

API neutron units

3.3 Lithology effect

Calibration curves in figs. 11 ÷ 13 and 17, 18 correspond to the porosities measured in limestones. When the other lithologies are concerned GOI gives the correction chart *[21]* reproduced in fig. 19.

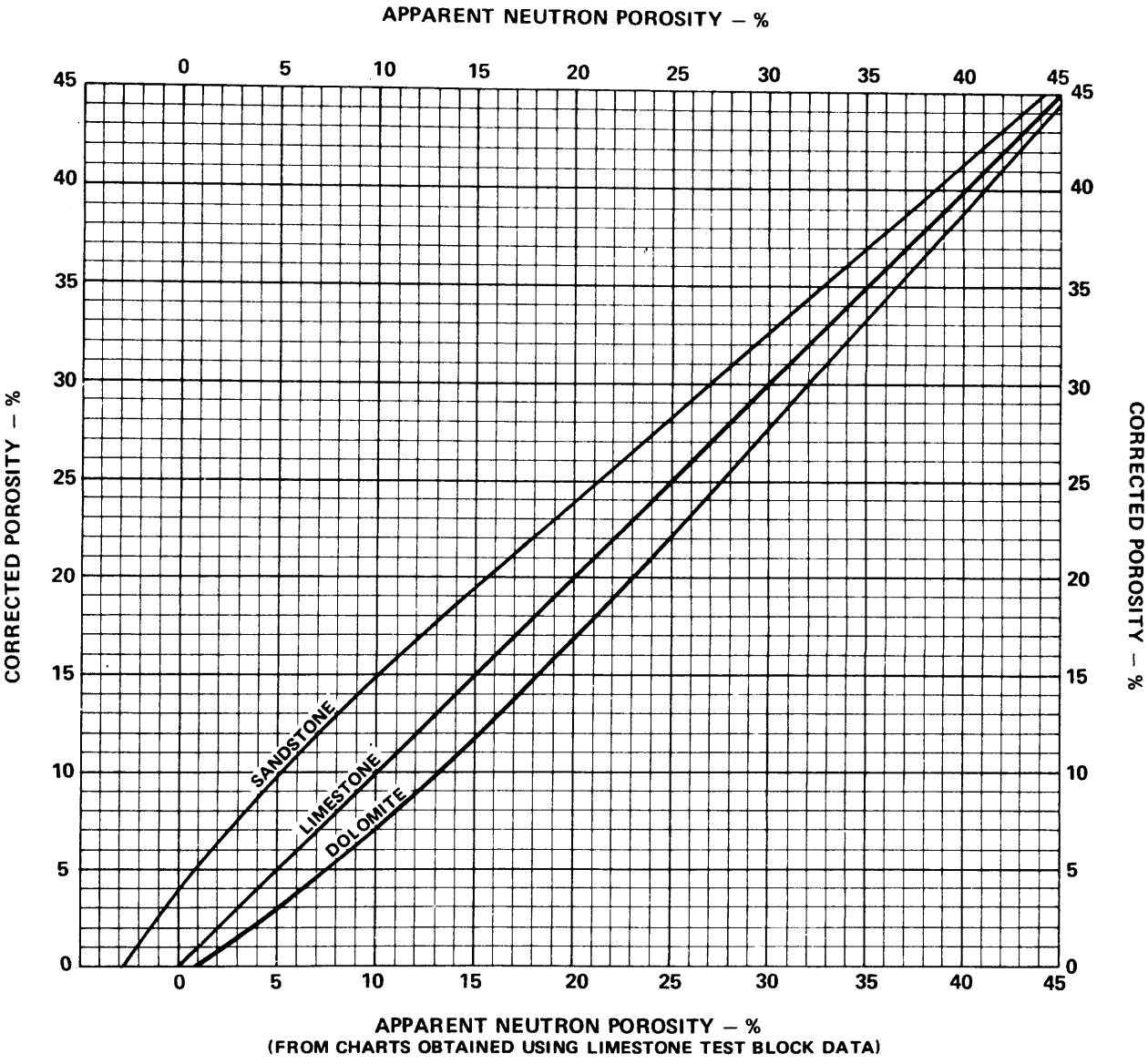

Fig. 19

Neutron porosity corrected for formation chemistry effects.

This chart has to be corrected now for the igneous rocks. Here the assumption of the chemical similarity of magmatic rocks to the sandstone formation is assumed (cf. § 3.1) and the influence of the rock apparent mineralogical density ρ_o will be taken into account. The following procedure, explained in fig. 20, is used:

The correction line for the igneous rock with ρ_o is sought. Let from the calibration curves the apparent limestone porosity is P_o. In fig. 19 through the point A one has the sandstone porosity P_1. Next, using the plots in figs. 7 or 8 for the porosity P_1 and for the apparent rock density $\rho_o = 2.65$ the point B is found which corresponds to the point C (the same L_s value!) when the apparent rock density is $\rho_o = 3.00$ - thus the porosity P_2 is found. In fig. 21 the apparent limestone porosity P_o and the corresponding porosity P_2 determine point D which is on the curve $\rho_o = 3.0$ just sought. Now, repeating this procedure for different values of P_o and ρ_o, the correction chart in fig. 21 is obtained.

As a result of interpretation in fig. 21 the so called true igneous rock porosity index (PI) is obtained by:

$$\Phi = \frac{PI - V_w}{1 - \frac{V_w}{100}} \; [\%] = \frac{PI - P_w \cdot \rho_M}{1 - \frac{P_w \cdot \rho_M}{100}} \; [\%] \qquad (31)$$

where

$$V_w = P_w \cdot \rho_M \qquad (32)$$

is the volume (in per cent of 1 cm^3) occupied by the chemically bounded water in the igneous rock of porosity $\Phi = 0\%$.

The entry in the plot of fig. 21 is the apparent limestone porosity and ρ_o. Apparent limestone porosity being known from the calibration curves, the ρ_o is obtained from eq. 21. To facilitate the calculations eq. 21 has been plotted in figs. 22 and 23 where the entries are the dry rock mineralogical density ρ_M and the weight (P_w) or volume (V_w) water content in the dry rock. The values ρ_M and P_w should be known from the laboratory analysis of the rock samples. For this reason it is necessary to collect the statistics of samples for a given type of igneous rock to obtain the average values ρ_M and P_w which can be used in this interpretation.

J.A. Czubek

Reykjavík, June 26, 1978

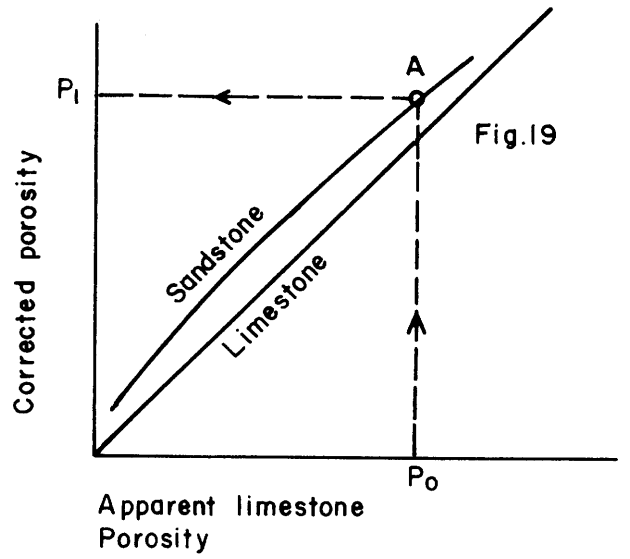
A
P1
Fig.19
Sandstone
Limestone
Corrected porosity
Po
Apparent limestone
Porosity

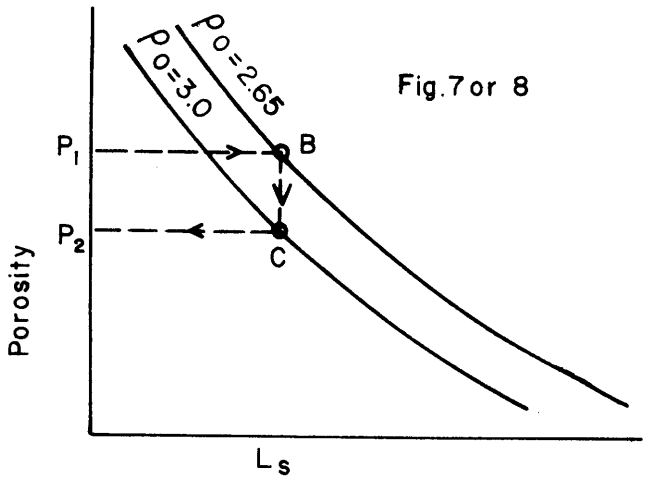
Po=2.65
Po=3.0
Fig.7 or 8
P1
B
P2
C
Porosity
Ls

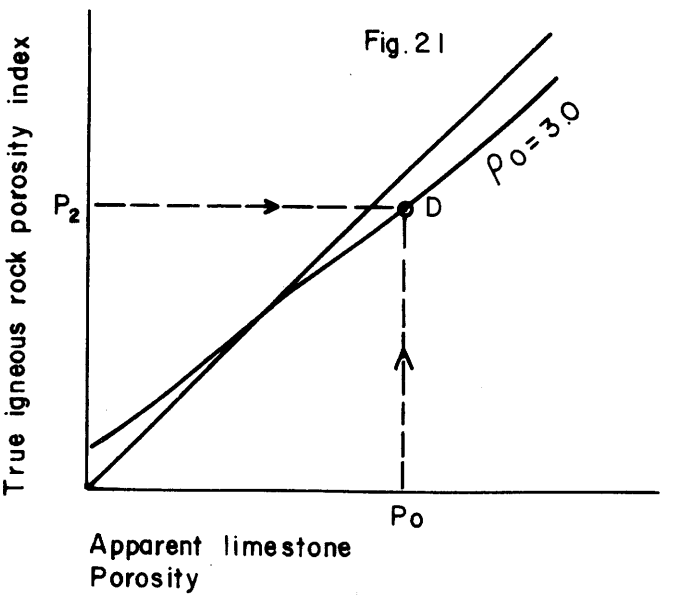
Fig. 21
Po=3.0
P2
D
True igneous rock porosity index
Po
Apparent limestone
Porosity

Fig. 20

Neutron porosity equivalence curves for igneous rocks
GOI 1"/16" neutron probe

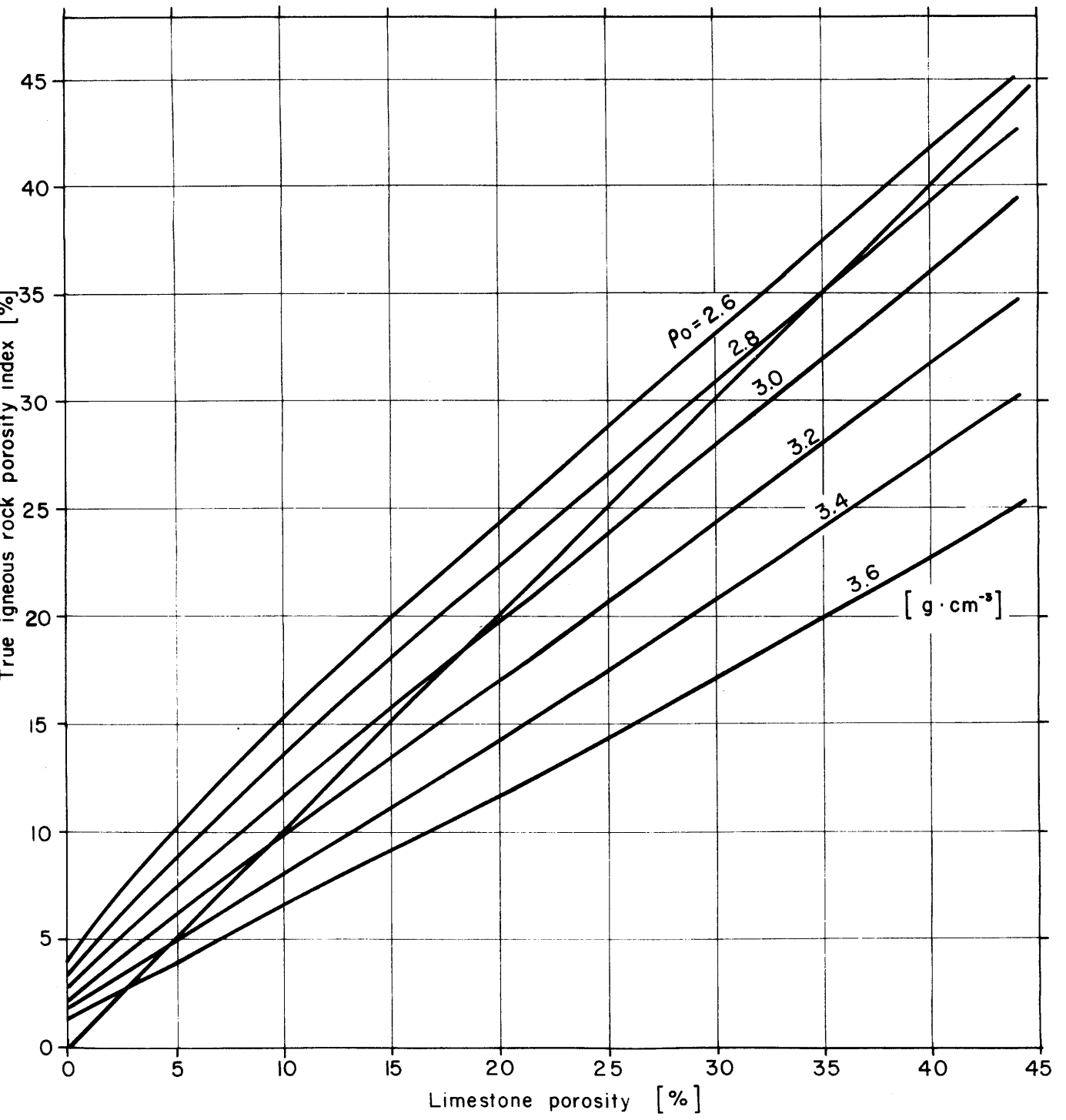

Fig. 21

Limestone porosity *[%]*

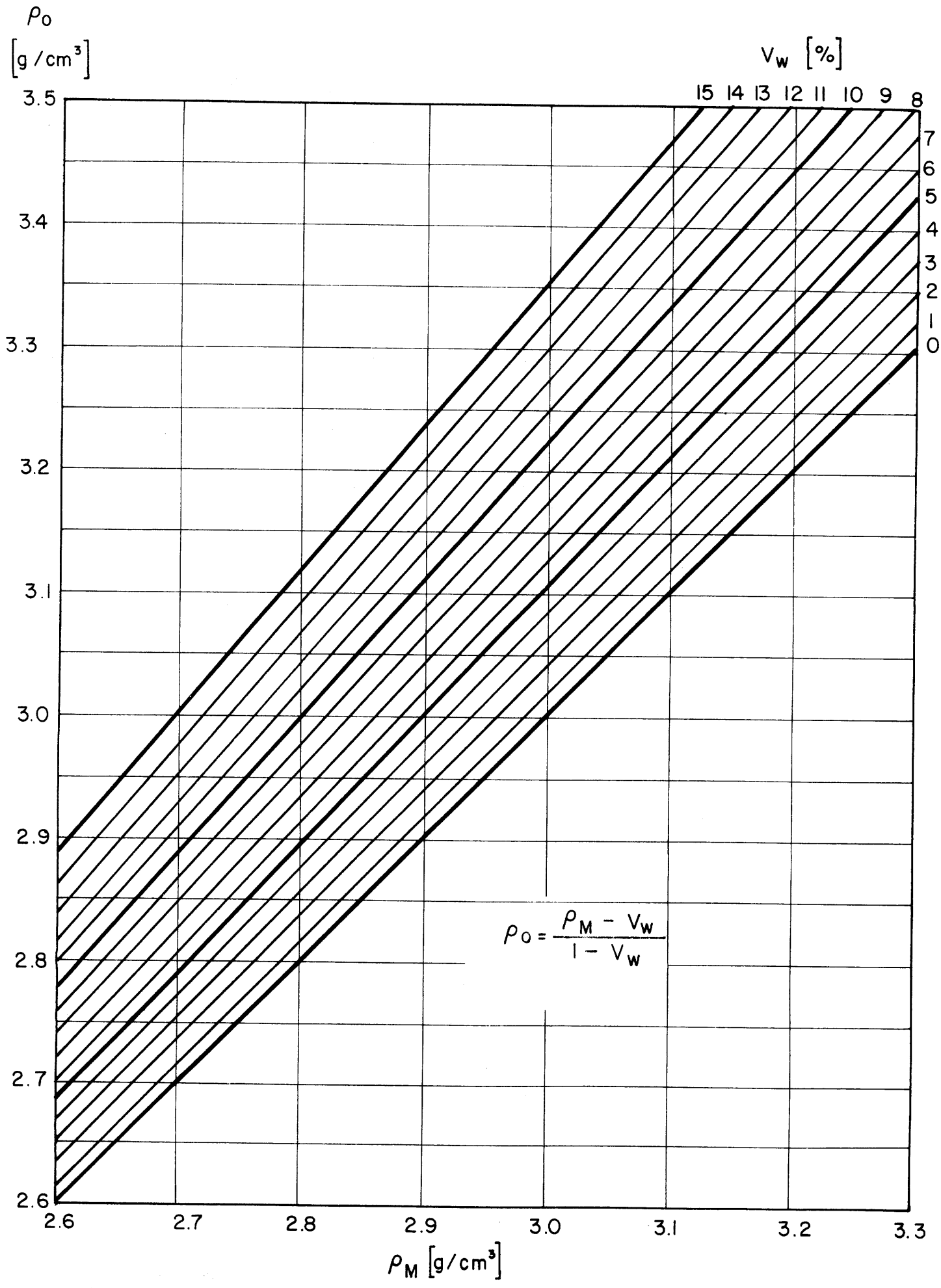
ρ_0 [g/cm³]
V_w [%]
15 14 13 12 11 10 9 8
7 6 5 4 3 2 1 0
3.5
3.4
3.3
3.2
3.1
3.0
2.9
2.8
2.7
2.6
2.6 2.7 2.8 2.9 3.0 3.1 3.2 3.3
ρ_M [g/cm³]
$\rho_0 = \frac{\rho_M - V_w}{1 - V_w}$

Fig. 22

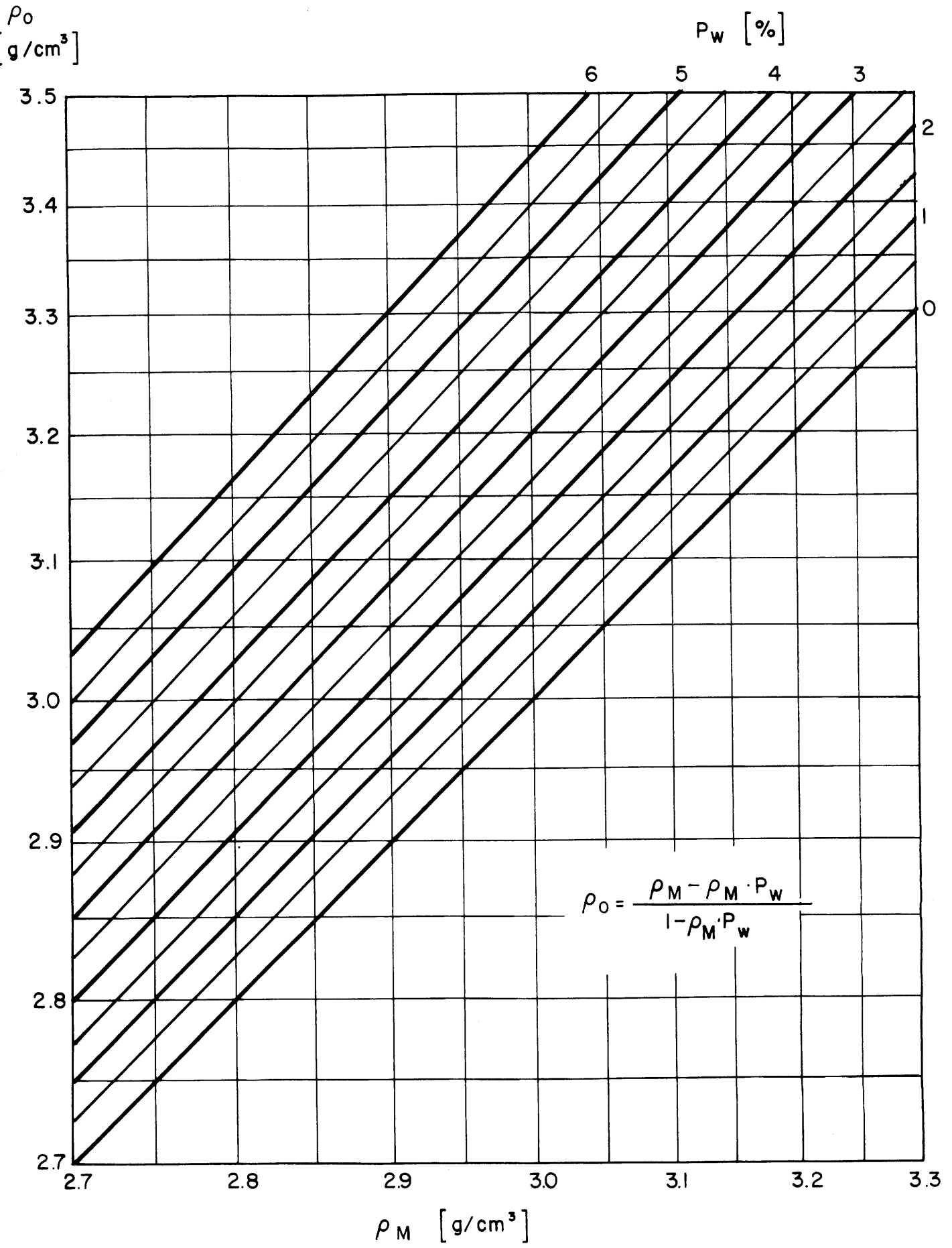
ρ_o [g/cm³]
P_w [%]
6
5
4
3
2
1
0
3.5
3.4
3.3
3.2
3.1
3.0
2.9
2.8
2.7
$\rho_o = \frac{\rho_M - \rho_M \cdot P_w}{1 - \rho_M \cdot P_w}$
2.7
2.8
2.9
3.0
3.1
3.2
3.3
ρ_M [g/cm³]

Fig. 23

REFERENCES [CHAPTER 3]

13. J.A. Czubek: Basic Physical and Theoretical Principles of Neutron Logging Methods. Melbourne 1975, manuscript, 75 p.

14. J.A. Czubek: Borehole Effects on Neutron Well Loggings. Melbourne 1975, manuscript, 34 p.

15. J.A. Czubek: Similitude Principles for Radiation Fields in Rocks. Density Method. Melbourne 1975, manuscript, 47 p.

16. J.A. Czubek: Similitude Principle for Neutron Fields in Rocks. Melbourne 1975, manuscript, pp. 48-88

17. A. Kreft: The Question of the Fast Neutron Absorption in Moisture Measurements by the Neutron Method. Nukleonika, 18 (1973) 615-623

18. A. Kreft: Calculation of the Neutron Slowing-Down Length in Rocks and Soils. Nukleonika, 19 (1974) 145

19. R.A. Daly: Igneous Rocks and the Depths of the Earth. McGraw-Hill Book Co., Inc. N.Y. and London 1933 (II-nd edition, 4-th impression), containing some revised chapters of "Igneous Rocks and Their Origin" (1914)

20. J.A. Czubek: Neutron Methods in Geophysics. Pp. 3-21 in "Nuclear Techniques and Mineral Resources", IAEA, Vienna 1969

21. GOI Formation Evaluation Data Handbook. Gearhart-Owen Industries Inc., Fort Worth, Texas 76101, October 1975

22. Schlumberger Log Interpretation Charts. Schlumberger Ltd., 1972 edition, U.S.A.